Marine and Petroleum Geology 155 (2023) 106345

Contents lists available at ScienceDirect

Marine and Petroleum Geology

journal homepage: www.elsevier.com/locate/marpetgeo

Concurrence of load-and-flame structures, balls-and-pillows, clastic injectites and shear deformation bands as indicator of seismicity in mixed siliciclastic-carbonate successions (Finale Ligure Basin, Italy)

Pierre Mueller [a,b], Silvia Tamburelli [a,*], Niccolò Menegoni [c], Michele Perozzo [a], Chiara Amadori [a], Laura Crispini [d], Laura Federico [d], Silvio Seno [a], Matteo Maino [a,e]

[a] Department of Earth and Environmental Sciences, University of Pavia, Pavia, Italy
[b] Lehr- und Forschungsgebiet Geotechnik und Tunnelbau, Technische Hochschule Köln, Köln, Germany
[c] Ali I. Al-Naimi Petroleum Engineering Research Center (ANPERC) - King Abdullah University of Science and Technology (KAUST), Saudi Arabia
[d] Department of Earth Environment and Life Sciences, University of Genoa, Genoa, Italy
[e] Institute of Geosciences and Earth Resources of Pavia, C.N.R, Pavia, Italy

ARTICLE INFO

Keywords:
Mixed siliciclastic-carbonate
Seismites
Clastic injectites
Deformation bands
Load-and-flame structures
Mediterranean basin
Basin tectonics
Ligurian alps

ABSTRACT

The present research explores a diverse suite of soft sediment deformation structures (SSDS) combined with clastic dykes and shear deformation bands distributed throughout a Early Miocene-age mixed carbonate-siliciclastic coastal wedge located on the Ligurian coast (NW Italy) of the Mediterranean region. The studied Aquitanian-Serravallian successions of the Finale Ligure Basin are typified by the presence of lithologically heterogeneous units, internally characterized by abrupt changes of lithofacies distributions and associated interpreted depositional environments. The interface between the terrigenous base and the carbonate wedge in many places features SSDS. Here, we report the discovery of a multiform deformational pattern, ranging from small size (cm-to dm-scale) load-and-flame structures, ball-and-pillows and mini-slumpings, to outsized (several meters in height) chaotic contorted and folded stratigraphic intervals, sand intrusions and diapir- or tree-like water escape structures. Many of the SSDS are related to fast injection of overpressurized fluids after sand liquefaction, and occur in close association with disaggregation and phyllosilicate shear bands, and sand dykelets. The stratigraphic distribution and cyclic repetitions of SSDS-prone intervals unambiguously indicates syn-depositional seismicity, thus suggesting that juxtaposition of SSDS, diapiric injectites, and shear deformation bands can serve as a suitable diagnostic criteria for seismite identification in the field. Since these particular assemblages of deformation structures reflect seismic activity in the area, they provide compelling evidence for previously undocumented tectonic episodes in Langhian-Serravallian times, associated with the latest stages of the Liguro-Provençal Basin opening.

1. Introduction

The origin of soft sediment deformations structures (SSDS) remains a disputed topic in clastic sedimentology, and unraveling their triggering mechanism is a challenging task in outcrop studies. SSDS are sedimentary structures related to both chemical and physical events. According to Mills (1983) the principal mechanisms responsible for this kind of deformation structures - alone or combined - comprise: (i) liquefaction or fluidization, (ii) reverse density gradation, (iii) slumping or slope failure and (iv) shear stress. It is important to note that those are the mechanisms of formation but not necessarily the trigger agents. The most common mechanisms resulting in SSDS development are fluidization and/or liquefaction, which typically develop both during sedimentation and/or shortly after deposition (e.g. Allen, 1982; Owen, 2003; Moretti and Sabato, 2007; Van Loon et al., 2020). SSDS typically form in water-saturated cohesionless sediments, as they result from significant decreases in shear resistance (Allen, 1982).

SSDS are not restricted to distinct depositional environments, as they have been documented in the entire range from proximal continental to abyssal marine realms (Shanmugam, 2017; Varejão et al., 2022). Continental occurrences include fluvial (Marshall, 2000; Went, 2005), volcanic (Smellie et al., 2006; Brown et al., 2007), lacustrine (Gruszka and

* Corresponding author. Department of Earth and Environmental Sciences, University of Pavia, via Ferrata 1, 27100, Pavia, Italy.
E-mail address: silvia.tamburelli01@universitadipavia.it (S. Tamburelli).

https://doi.org/10.1016/j.marpetgeo.2023.106345
Received 17 February 2023; Received in revised form 29 May 2023; Accepted 30 May 2023
Available online 5 July 2023

Van Loon, 2007), and eolian depositional environments (Horowitz, 1982; Moretti, 2000). SSDS have moreover been documented in glacial and periglacial settings (e.g. Le Heron et al., 2005; Brandes et al., 2012, 2018a), where ice-sheet loading, glacio-tectonism, and freeze-and-thaw processes represent important triggers for SSDS (Van Loon et al., 2020). Transitional continental-marine domains may also feature SSDS, essentially in deltaic environments (e.g. Hickson and Lowe, 2002; Ekwenye et al., 2020). Marine environments prone to SSDS range from tidally-influenced (e.g. Greb and Archer, 2007), over shallow marine (Molina et al., 1998), to deep-water settings (e.g. Chen et al., 2019; Oliveira et al., 2009).

Although a range of processes can lead to SSDS formation, the main triggering factors are overloading or unequal loading (i.e., density-driven deformation that arises from differences in bulk density of the involved strata), wave-induced stresses (both cyclical and impulsive), sudden changes in groundwater level, and earthquake-induced seismicity (e.g. Seilacher, 1969; Mills, 1983; Obermeier, 1996; Van Loon, 2009; 2009; Moretti and Sabato, 2007; Owen et al., 2011; Brandes and Winsemann, 2013; Shanmugam, 2017). Resultant fluid escape structures are interpreted as related to (i) earthquake shock (cyclic and concentrated) or (ii) nearly instantaneous deposition or altered groundwater movements (Mills, 1983). Earthquakes can affect surficial layers by sudden changes in pore-water pressure. Particularly silty and sandy layers with a high content of clayey material are subjected to hydroplastic deformation (Van Loon, 2009), although even gravels may be affected (Carter and Norris, 1986). The style and intensity of deformation can range from slight to chaotic, culminating in complete disruptions of affected strata. Deformation-prone strata may show a wide variety of SSDS, ranging from deformation bands to hydroplastic folds such as convolutions, load casts and flame structures (Moretti and Sabato, 2007). To this date, the exact discrimination of the trigger process of SSDS however remains problematic, essentially based on the exclusion of the influence of other triggering mechanisms (Owen et al., 2011; Shanmugam, 2017; Varejão et al., 2022). Notwithstanding, deformation bands in unconsolidated sediments are considered robust indicator for syn-depositional activity (either seismic and slow creep) of deep basement faults (Cashman et al., 2007; Brandes and Tanner, 2012; Shipton et al., 2017; Brandes et al., 2018a, 2022).

In this paper, we present the first documentation of disturbed sediments in the mixed carbonate-siliciclastic sedimentary successions of the Finale Ligure Basin (Issel, 1892; Boni et al., 1968; Dallagiovanna et al., 2011; Brandano et al., 2015; Della Porta et al., 2022), which crops out along the Ligurian coast, in the northern part of the Western Mediterranean region (Fig. 1). The Finale Ligure Basin represents an upper Oligocene to middle Miocene coastal wedge that unconformably overlies metamorphic units of the Ligurian Alps (Brandano et al., 2015, 2022; Della Porta et al., 2022). It is constituted by a basal terrigenous sequence, which is superimposed by the Pietra di Finale carbonate sequence. In particular the interface between the terrigenous and calcareous sequences is defined by intercalated sedimentation patterns. It displays exceptionally well-exposed SSDS, mainly represented by load-and flame structures and ball-and-pillow structures, fluid-driven upward expulsion of strata of the lower clastic unit, and the presence of deformations bands.

SSDS in carbonate successions are comparatively understudied in comparison to their widely documented siliciclastic counterparts (Bourli et al., 2020). In view of the recent increase of importance of mixed siliciclastic-carbonate successions as exploration targets (e.g. Chiarella et al., 2017; Du et al., 2022; Hussain et al., 2022), and the fact that SSDS and deformation bands can create heterogeneity in sub-surface

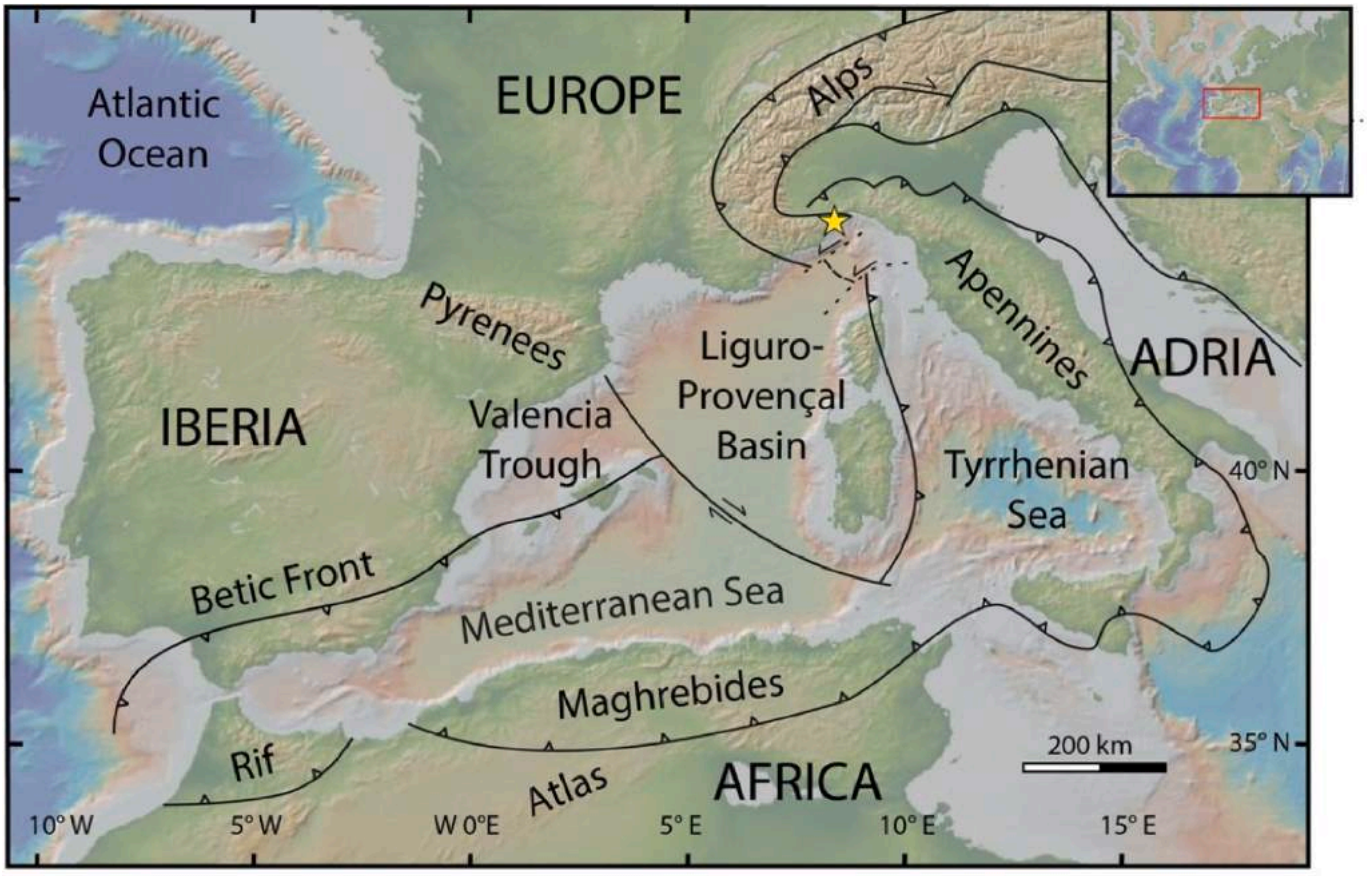

Fig. 1. Simplified tectonic sketch of the Western Mediterranean region (modified from Faccenna et al., 2004; Oudet et al., 2010). The yellow star indicates the location of the Finale Ligure Basin.

reservoirs (e.g. Sternlof et al., 2004; Farrell et al., 2014; Fossen et al., 2018) and CO_2 storage sites (Warsitzka et al., 2017), this study aims at investigating the nature, origin and impact of SSDS in poorly studied mixed settings. Moreover, due to the lack of any deformation evidence - including seismic record - the Finale Ligure Basin has traditionally been considered as a low-strain domain (Boni et al., 1968; Dallagiovanna et al., 2011), although it developed during a phase of tectonic reorganization of the Western Mediterranean region, driven by the opening of the Liguro-Provençal basin (Fig. 1).

A multi-method approach ranging from micro-to outcrop-scales comprises: (i) a detailed study of the sedimentological and structural characteristics at the outcrop-scale; (ii) photogrammetric investigations of the geometry of the structures and their stratigraphic occurrence and (iii) petrographic and textural analyses. This descriptive approach gives insights into the pivotal role of fluids as promoter of deformation, intrastratal sediment mobilization and solution/cementation processes. Given the regional stratigraphic and tectonic framework, the final aims of this study are: i) to unravel the origin of atypically large SSDS within a mixed siliciclastic-carbonate succession; ii) distinguishing between autogenic and allogenic processes as possible triggering forces; iii) test the concurrent presence of multiform SSDS, clastic dykes and shear deformation bands as a diagnostic tool for determining seismites; and iv) to constrain seismic activity during a major tectonic re-organization of the central Mediterranean area during the Early Miocene.

2. Geological background

2.1. Tectonic setting

The Finale Ligure Basin reflects a major transgression marked by the deposition of mixed siliciclastic and carbonate sediments in a confined embayment setting, inherited from the marine flooded Alpine bedrock (Boni et al., 1968; Della Porta et al., 2022). It is located in the Ligurian Alps (Figs. 1 and 2A), which represent the junction between two arch-shaped orogenic belts, the Western Alps and the Apennines (Vanossi et al., 1986; Seno et al., 2005; Maino et al., 2013). The Ligurian Alps are formed by imbricated tectonic units derived from three pre-Alpine paleogeographic domains: the Briançonnais, Pre-Piedmont and the Piedmont-Ligurian oceanic domains (Bonini et al., 2010; Maino and Seno, 2016; Mueller et al., 2020). While the Briançonnais and Pre-piedmont domains represent the European continent and its margin, the Piedmont-Ligurian domain is composed of oceanic crust and its pre-collisional sedimentary cover (Seno et al., 2003; Mueller et al., 2020). Below the Finale Ligure Basin, the metamorphic basement consists of Briançonnais units which experienced subduction- and collision-related metamorphism and deformation from late Eocene to early Oligocene times (Vanossi et al., 1986; Bonini et al., 2010; Maino et al., 2012, 2015a, 2015b, 2020). In response to the Apennines' northeastward migration and the inception of the Ligurian-Provençal back-arc basin opening (~35-30 Ma; de Voogd et al., 1991; Rollet et al., 2002), the Ligurian Alps and the associated retro-wedge basin (i.e., the Tertiary Piedmont Basin) record Early Oligocene extensional followed

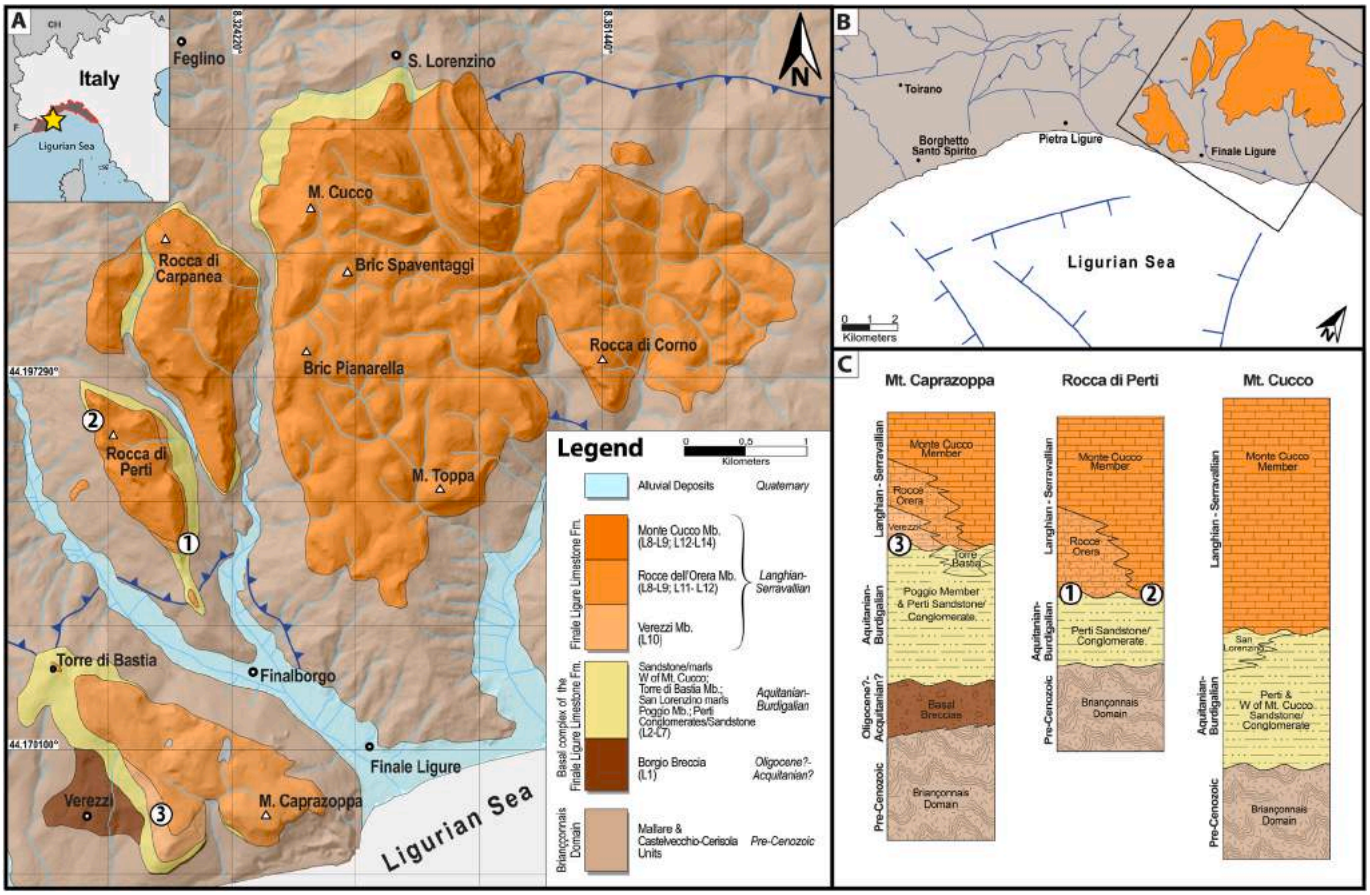

Fig. 2. A) Geological map of the Finale Ligure Basin (redrafted after Boni et al., 1968 and new mapping) along the Ligurian coast in NW Italy (insert in the upper left corner). Stratigraphic units of the legend are from Boni et al. (1968); note that Perti sandstone and conglomerate refers to "Bracciale, Perti, Ansaldo, Costa and Rocca degli Uccelli conglomerate and sandstone" of Boni et al. (1968). B) Tectonic sketch of the Ligurian coast comprising the Finale Ligure Basin (in orange),highlighting the main fault network in the continental basement and offshore (from Dallagiovanna et al., 2011; Maino et al., 2013; Morelli et al., 2022). C) Stratigraphic logs of representative succession of the Finale Ligure Basin. Numbered circles indicate the positions of the three localities where SSDS were studied.

by Late Oligocene transtensional faulting episodes (Maino et al., 2013; Decarlis et al., 2014; Federico et al., 2020; Amadori et al., 2023), combined with transpressional to compressional faulting in central Liguria (Federico et al., 2014; Crispini et al., 2009). Since the Miocene, spatially and temporally alternating extensional and compressional phases are documented (Maino et al., 2013; Morelli et al., 2022). The Liguro-Provençal ocean spreading reached climax in the Langhian-Serravallian (Speranza et al., 2002), when rotation of the Ligurian Alps accommodated the rifting phase, as well as eastward drifting of the Corsica-Sardinia block (Vanossi et al., 1994; Gattacceca et al., 2007; Maffione et al., 2008; Maino et al., 2013). Drifting was accomplished in the Ligurian Sea through extensional tectonics, while the post-drifting evolution is characterized by episodic tectonic inversions from extension to transpression during Serravallian-Messianian times, and since the Pliocene to present (Larroque et al., 2011; Morelli et al., 2022).

2.2. Stratigraphy

2.2.1. Pre-tertiary basement

The pre-Tertiary basement of the Finale Ligure Basin is represented by the Briançonnais Mallare and Castelvecchio-Cerisola units (Seno et al., 2005; Maino et al., 2012a). They comprise i) Permian meta-sedimentary and -volcaniclastic successions (Dallagiovanna et al., 2009; Maino et al., 2012b; 2019) and ii) a Meso-Cenozoic sedimentary sequence that comprises fluvial Lower Triassic metaconglomerates and quartzites, Middle Triassic platform carbonates and dolostones, Upper Jurassic marbles and Upper Cretaceous calcareous schists (Decarlis et al., 2013, 2014, 2017; Seno et al., 2005).

2.2.2. Stratigraphy of the Finale Ligure Basin

The pre-Tertiary basement is unconformably covered by a siliciclastic post-orogenic basin fill, superimposed by a thick mainly carbonatic sequence. The stratigraphic definition of these deposits evolved trough times. In the first descriptions (Fig. 3; Boni et al., 1968, 1971; Mosna et al., 1990), the Finale Ligure Basin sequence has been subdivided into two lithostratigraphic units, including: the "Finale Ligure Limestone" (Calcare di Finale Ligure; "Pietra di Finale" *Auct.*) and the "Tertiary Substrate" or "Basal Complex of the Finale Ligure Limestone" ("Substrato Terziario" or "Complesso di base dei Calcare di Finale Ligure" *Auct.*). While the presence of a carbonate sequence is limited to the upper unit, the terrigenous deposits are present in both. The siliciclastic sediments are represented by a monogenic breccia, polygenic conglomerates and sandstones, marlstones and siltstones. In between the individual members, they display abrupt vertical and lateral transitions in terms of facies and style of deposition. Their stratigraphic relationships are often difficult to reconstruct because of discontinuous outcrop exposures and the scarcity of fossil content in most of the breccias, conglomerates and sandstones (Boni et al., 1968, 1971; Mosna et al., 1990). The lower unit – the "Tertiary Substrate" or the "Basal Complex of the Finale Ligure Limestone" - includes four siliciclastic members (Figs. 2 and 3): 1) monogenic breccias with clasts of Triassic dolostones ("Borgio Breccia" *Auct.*); 2) polygenic conglomerates and sandstones ("Bracciale, Perti, Ansaldo, Costa and Rocca degli Uccelli conglomerate and sandstone" *Auct.*); 3) grey-yellow claystones, siltstones and marlstones ("S. Lorenzino Marls" *Auct.*); 4) coarse sandstones and fine-grained, quartz-rich conglomerates with centimeter-thick intercalations of green claystone and marlstone ("Sandstones and Marls, West of Mt. Cucco" *Auct.*). The age of these deposits is suggested to be early Oligocene (Mosna et al., 1990) to possibly Aquitanian-Burdigalian for the Marls West of Mt. Cucco (Boni et al., 1968, 1971). The upper formation - the "Finale Ligure Limestone" - includes two siliciclastic and three carbonate members that show heteropic sedimentation patterns (Figs. 2 and 3): 1) polygenic conglomerates and sandstones ("Poggio Mb." *Auct.*); 2) marlstones, sandstones, intercalated with packstone-wackestone ("Torre di Bastia Mb." *Auct.*) attributed to

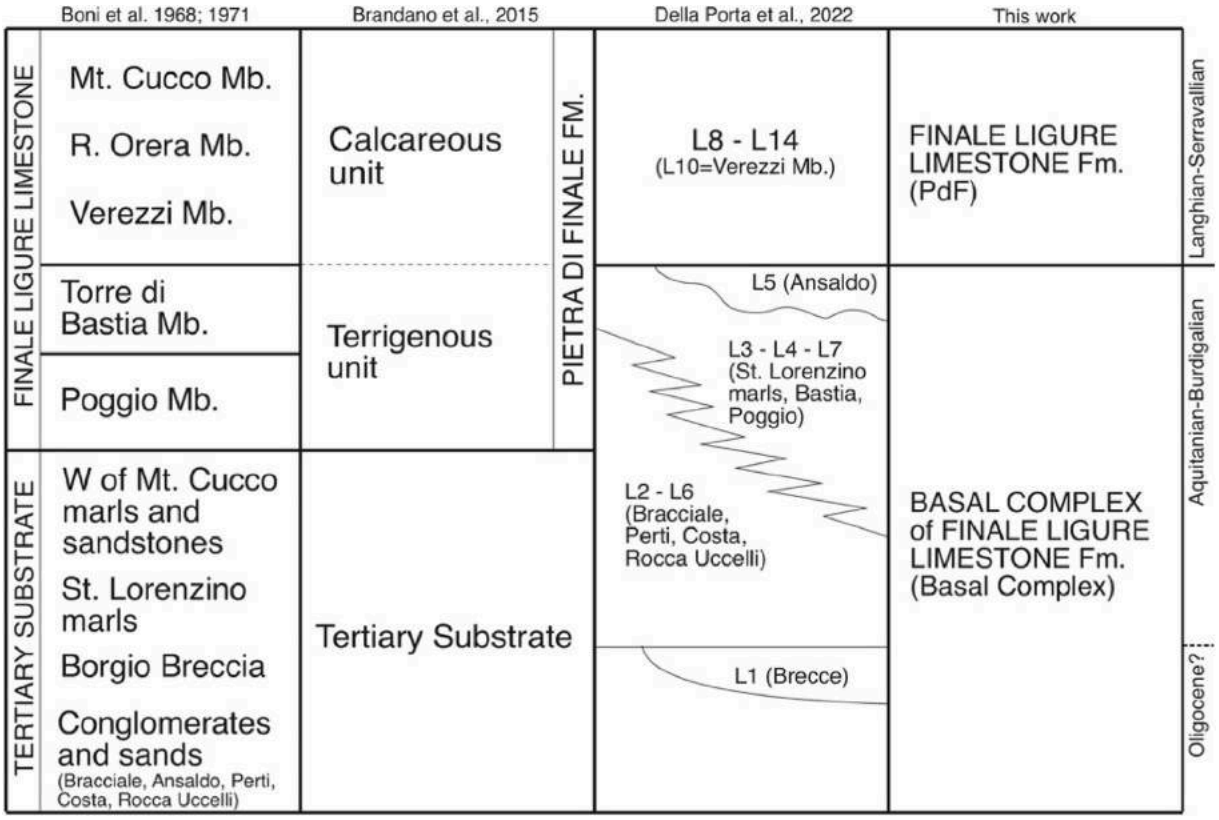

Fig. 3. Comparison of lithostratigraphic subdivisions of the Oligocene?-Miocene sedimentary succession of the Finale Ligure Basin deposited on the Alpine metamorphic basement according to different authors, included the one proposed in this work.

Aquitanian-Burdigalian to probably basal Langhian age (Boni et al., 1968); 3) red-color skeletal calcarenites associated with siliciclastic detrital grains ("Verezzi Mb." *Auct.*); 4) hybrid arenites interbedded with polygenic conglomerates ("Rocce dell'Orera Mb." *Auct.*); 5) skeletal limestones with scarce terrigenous fraction ("Monte Cucco Mb." *Auct.*). On the basis of the abundant fossil content, the carbonate members are attributed to Langhian-Serraviallian times (Boni et al., 1968; Mosna et al., 1990).

Brandano et al. (2015) confirmed the stratigraphic description of the lower unit (i.e., "Basal Complex" of the Finale Ligure Limestone), but recall the "Finale Ligure Limestone" into "Pietra di Finale Fm.", dividing it in into a terrigenous unit (comprising the "Poggio and Torre di Bastia Mbs.") and a calcareous unit corresponding to the "Verezzi, Rocce dell'Orera and Mt. Cucco Mbs" (Fig. 3).

Della Porta et al. (2022) provide a detailed description of fourteen lithofacies (L1 to L14; Fig. 3), where the basal L1 to L7 are terrigenous, corresponding with the lower unit of Boni et al. (1968, 1971) ("Basal Complex" of the Finale Ligure Limestone), together with the two lowermost members of the "Finale Ligure Limestone" ("Poggio and Torre di Bastia Mbs."; i.e. the terrigenous unit of Brandano et al., 2015). Lithofacies L8 to L14 belong to the calcareous members of "Finale Ligure Limestone" of Boni et al. (1968) ("Verezzi, Rocce dell'Orera and Mt. Cucco Mbs."; i.e., the calcareous unit of Brandano et al., 2015).

The stratigraphic units of Boni et al. (1968) and (1971) have been formalized in the Italian geological mapping project (CARG) into two formations (Dallagiovanna et al., 2011): the *Basal complex of the Finale Ligure Limestone Fm.* (hereafter Basal Complex) and the *Finale Ligure Limestone Fm.* ("Pietra di Finale", hereafter PdF). Biostratigraphic investigations accomplished in the framework of the CARG project suggest a revision of the depositional age of the "San Lorenzino Marls" ranging from Oligocene (Giacomini, 2009; Dallagiovanna et al., 2010, 2011) towards Aquitanian times. Therefore, apart from few undated basal breccias and conglomerates lacking fossil content, most of the siliciclastic sediments are Aquitanian-Burdigalian in age.

2.2.3. Lithofacies characterization and spatial distribution

The lower part of Basal Complex crops out in the southwestern part of the Finale Ligure area (Mt. Caprazoppa section of Fig. 2C), and is represented by up to 100 m thick breccias predominantly consisting of dolomite clasts. They locally display lenticular bed-set geometries and ("Borgio Breccia" of Boni et al., 1968; cf. L1 of Della Porta et al., 2022), and are interpreted to represent proximal channelized colluvium deposits (Mosna et al., 1990). Laterally to this breccia, up to 15 m thick alternations of coarser polygenetic siliciclastic and finer marly intervals display rapid lateral facies changes ("Bracciale sandstone and conglomerate" of Boni et al., 1968; L2 of Della Porta et al., 2022). The composition of the sandy deposits widely matches that of the Permian volcano-clastic Briançonnais deposits, which, together with high textural maturity and the presence of echinoid fossils, suggests deposition in fluvial to deltaic environments (Mosna et al., 1990). Above both conglomerates and breccias, coarse sandstones and polymictic microconglomerates of the "Poggio member" (Boni et al., 1968; L7 of Della Porta et al., 2022) are mainly composed of dolomitic clasts. This member reaches a maximum thickness of ca. 50 m. While the basal part of the succession (ca. 10 m in thickness) features massive sandstones, a coarsening-upward trend into more organized, well-stratified conglomeratic strata typifies the stratigraphic organization of the member. Sediments show high textural maturity and abundant calcite cement. Bivalve imprints are common. Subordinate echinoid fossils are present. The "Poggio conglomerates" shows lateral heteropy with several facies of the "Torre di Bastia Mb." (Boni et al., 1968; L3 of Della Porta et al., 2022). The "Torre di Bastia Mb." reaches a cumulative thickness of ca. 60–70 m. It comprises a basal interval typified by alternations of thin sandstone beds and greenish-yellow clays. The marl-prone upper parts comprise sandy marls, which show an up-section gradual transition into marls enriched in calcite. Sedimentary facies suggest a wide range of depositional environments. A recent re-investigation of the microfaunal assemblages of the "Torre di Bastia Mb." indicates a early Burdigalian depositional age (i.e., BA3-BA4 of the IFN3 biozone; cf. Giacomini, 2009; Dallagiovanna et al., 2010, 2011). Silicified volcaniclastic sandstones and conglomerates are intercalated into the topmost marly horizons of the "Torre di Bastia Mb.", with the coarser grained strata typically displaying erosional basal contacts (Vanossi, 1991). Eastward, the Rocca di Perti section (Fig. 2c) is characterized by up to 40 m thick polygenetic litharenites and conglomerates, hosting channel incision filled of m-sized clasts ("Perti sandstone and conglomerate" of Boni et al., 1968; L6 of Della Porta et al., 2022). In the northern part of the Finale Ligure Basin (Mt. Cucco section, Fig. 2c), the sequence begins with alike 10 m thick polygenetic clastic sediments ("Costa conglomerates and sandstones" of Boni et al., 1968), overlain by up to 20 m thick hemipelagic marls ("Monte Cucco and San Lorenzino Marls" of Boni et al., 1968; L4 of Della Porta et al., 2022). They comprise litharenites which alternate with claystone beds rich in microfaunal assemblages that yield Aquitanian age (Giacomini, 2009; Dallagiovanna et al., 2010, 2011). In their upper parts both marly members show repeated incisions of sandstone- and conglomerate-filled bodies. An erosional unconformity separates the top of the "San Lorenzino marls" from a ca. 3 m thick layer of structureless quartzose sandstones and conglomerates ("Ansaldo sandstone" of Boni et al., 1968; L5 of Della Porta et al., 2022), which alternate with thin heterolithic intervals consisting of thin-bedded, very fine grained strata (Mosna et al., 1990).

Based on macrofossil findings, the deposition of the overlying bioclastic limestones that form the PdF can be constrained to Langhian to Serravallian ages (Boni et al., 1968; Brandano et al., 2015). The "Verezzi member" (L10 of Della Porta et al., 2022) is represented by grainstone lithologies composed of green calcareous algae limestones that comprise abundant shells, minor portions of echinoid fossils, and rare occurrences of isolated corals, brachiopods, oysters and fish teeth (Boni et al., 1968). Average thickness of the well-bedded, reddish calcarenitic strata is ca. 0, 3–0,5 m. The "Verezzi member" reaches a maximum thickness of ca. 50 m (Boni et al., 1968; Della Porta et al., 2022). The overlying "Rocce d'Orera member" (L8-9, 11–12 of Della Porta et al., 2022) is represented by massive, highly porous bioclastic limestones that generally comprise terrigenous components. Main bioclastic components are fragments of corals, algae, molluscs, bryozoans, and balanids (Boni et al., 1968; Della Porta et al., 2022). Throughout the stratigraphic section, the succession shows intercalations of sandstones and conglomerates similar to those of the "Poggio Mb." (Mosna et al., 1990), reaching a maximum thickness of ca. 40–70 m (Brandano et al., 2015; Della Porta et al., 2022). The "Monte Cucco Mb." (L8, 12–14 of Della Porta et al., 2022) forms the distinctive cliffs of the PdF. Locally, terrigenous marly to coarse sandy intervals mark the basal contact between the "Monte Cucco member" which in that case directly superimposes the "Torre di Bastia member" (Boni et al., 1968). Lithologically, the "Monte Cucco Mb." is represented by bioclastic limestones with very minor non-skeletal proportions. The principal skeletal fraction is that of *Hydrozoan* debris (Boni et al., 1968; Brandano et al., 2015, 2022; Della Porta et al., 2022). Intervals characterized by abundant inorganic content comprise balanids, bryozoans, and pelecypod skeletal remains. The member reaches a maximum thickness of up to 200 m and has been interpreted to be deposited in an enclosed and shallow marine environment (Boni et al., 1968; Brandano et al., 2015), or, more recently, to a narrow strait defined by intermittent to high-energy bottom currents (Della Porta et al., 2022).

Paleo-environmental conditions during time of deposition of the exclusively carbonate members have been explored by Brandano et al. (2015), who proposed constraints on climatic conditions and nutrient availability that controlled the carbonate factory during Langhian-Seravallian times (i.e., the "Verezzi, Rocce dell'Orea and Monte Cucco Members"). The most recent studies on the PdF further explore energetic controls on the carbonate buildup (Brandano et al., 2022), and provide new insights into paleo-environmental conditions such as hydrodynamic energy, nutrient availability, and basin

configuration (Della Porta et al., 2022), both suggesting high-energy conditions within a wave-dominated scenario.

3. Methodology and dataset

Fieldwork was performed through extensive mapping at the 1:10 000 scale in the framework of the Italian geological mapping project (CARG "Foglio 245-Albenga"). Field observations were acquired at the outcrop scale, aimed at exploring individual contacts between different lithofacies, as well as the potential presence of deformation structures. A reconsideration of the boundary between the Basal Complex and the PdF (Fig. 3) was carried out, streamlining the pioneering lithostratigraphic scheme of Boni et al. (1968) and the recent updates of Brandano et al. (2015) and Della Porta et al. (2022).

Field data has been augmented with orthophoto-panels and DOMs acquired via drone imagery. Orthophoto-panels were generated through a DOM approach (Menegoni et al., 2022), comprising acquisition of more than 2000 photographs with mean resolution of around 3 mm/pixel using a quadcopter DJI Phantom 4 RTK, the DOM development and the extraction of orthorectified images with point of views that best-fit SSDS.

Sedimentological investigations of SSDS-prone interfaces were conducted at three main localities. Study locations are illustrated in Fig. 2B, and their stratigraphic positions are shown in Fig. 2C. Detailed sedimentary facies analyses of the studied sediments are provided by the recent works Brandano et al. (2015, 2022) and Della Porta et al. (2022).. We base our findings and interpretations on this framework. Sedimentological analysis was performed with emphasis on the sedimentary facies of strata incorporated into SSDS-prone interfaces, and in-depth description of character and morphology of deformational features. Analysis of deformed strata aimed at exploring lithology, bed or bed-set thickness, primary sedimentary structures, granulometry, and nature of bed bounding surfaces. Sediment-grain size was determined in the field with a hand lens and a standard grain size chart In case of some large deformation structures that ,comprise poorly consolidated sediments granulometric data was further acquired according to the DIN EN ISO 17892-4 standard, utilizing the mechanical sieving and hydrometer analyses (Kolmar and Cui, 1984). Grain size measurements have moreover been conducted on thin sections utilizing the ImageJ software (Rasband and ImageJ,). Porosity of representative deformation domains have been acquired through optical petrography of thin sections impregnated with blue epoxy resin. After sample scanning, pore spaces have been estimated following the procedure of Rabbani et al. (2017). Paleocurrent orientations were analyzed by measuring the orientation of ripple fore-sets. Lateral changes in sedimentary facies, granulometry, and style of juxtaposed deformation features were documented by means of walking out interfaces that exhibit SSDS. Categorization of loading structures was conducted according to the descriptive criteria of Owen (2003). Classification of upward-direct deformations (i.e. flame structures and clastic dykes) was performed following the proposed scheme of Oliveira et al. (2009). Structural investigations are based on recognition and attitude measurements of fractures, faults and shear bands. Particular emphasis has been devoted to deformation shear bands as they allow identification of deformation of unconsolidated sediments. The structural dataset was subsequently synthetized into classic stereographic projections.

4. Results: descriptions of SSDS at study locations

4.1. Study location 1: Basal Complex (Perti village)

The studied exposure at location 1 (Perti village; Fig. 2) comprises a basal, relatively thick (ca. 2 m) marly layer within the "Perti conglomerate and sandstone" lithozone of the Basal Complex (L6 of Della Porta et al., 2022), that is superimposed by a thick (>10 m of vertical outcrop exposure) succession of coarse sandstones and polymictic conglomerates. Marls display faint cross-bedding, while the coarser sediments are massive, lacking primary sedimentary structures (Fig. 4A). A range of SSDS can be observed at the interface between the marls and their superimposing coarse counterparts. The contact between the light brownish marls and the coarser sediments is generally sharp. Lateral outcrop exposure is ca. 50 m. The most abundant type of SSDS are load casts. They are distributed along the entire lateral exposure of the outcrop, resulting in an overall undulating interface (Fig. 4A). Load casts typically display asymmetric, concave-up shapes. They downward intrude into the thick marly interval that locally shows discontinuous, very thin fine sandy interbeds. Load casts have lateral extensions of up to ca. 1.2 m and depths of up to 45 cm (Fig. 4A). Locally, flame structures can be found, typically associated with lateral terminations of load casts. They are characterized by upward-directed intrusions of marly substrate into the coarse sandy overlying bed (white arrows in Fig. 4A). Flames are asymmetric, and in some cases flame tips show a tendency of down-dip (i.e. S-SW) orientations. Maximum flame dimensions are 12 x 3 cm. Another distinctive feature of the exposure is the presence of sub-vertical, upward-oriented dyke (i.e., laccolith-shaped) structures, located at the lateral terminations of huge load casts. Their upper terminations show cusp-to x-shaped morphologies (Fig. 4 B, C). Their dimensions range from a height of 75 cm and a width of 55 cm to a maximum height of 110 cm and a width of 80 cm, respectively.

The marly interval moreover features a variety of pseudonodules, which can be subdivided into large, detached ball-and-pillow structures (Fig. 4B), and smaller, attached and well-rounded ovoid to ball-shaped structures (Fig. 4E). Large ball-and-pillow structures show elongated, kidney-shaped morphology, and typically display rounded to sub-rounded edges (Fig. 4A). Maximum dimensions are 65 x 30 cm. The ball-and-pillow structures (i.e. pseudonodules) are composed of medium sand, and lack evidence of internal grading. They are distributed in the underlying marly substrate and typically occur in horizontal alignments along a distinct horizon located ca. 25–40 cm below the interface (Fig. 4A). The well-rounded, smaller ovoid and locally ball-shaped varieties comprise pseudonodules with a maximum diameter of 12 cm. Average grain size is medium to coarse sand. They form clusters of closely aligned individual small pseudonodules, with a thin marly matrix separating each pseudonodule from its neighboring equivalents. From top to base of the structure, a general trend in reduced maximum diameters can be observed (Fig. 4D). These accumulations are v-shaped, and show sub-vertical orientation. Maximum downward vertical extension is ca. 80 cm. At its topmost exposure the accumulation shows its broadest width of ca. 45 cm. In addition, a single specimen of an isolated small nodules was encountered in a marly-sandy interval that displays remnant cross-bedding (Fig. 4E).

4.1.1. Interpretation of the SSDS

Sedimentological analysis reveals that the interface between marls and sandstones of the *Basal Complex of the Finale Ligure limestone* from location 1 (Perti village; Fig. 4B, C, Fig. 4A–E) is dominated by the presence of loading structures such as simple load-and-flame structures. Clastic injectites, and – to a minor degree –pseudonodules represent less common forms of SSDS. We interpret these SSDS as originated from the presence of a marked density contrast in between the fine-grained marly sediments and their overlying coarse-grained counterparts (Fig. 13A), which both form part of the Perti Sandstones and Conglomerates (L6 of Della Porta et al., 2022). The characteristic bulbous shapes of the load casts would point towards depositional loading as the cause of deformation recorded in the topmost part of the marly horizon (Owen, 2003; Van Loon and Pisarska-Jamroży, 2014). Flame structures are interpreted to equally reflect gravitational loading of the thick packages of dense sediment onto the underlying less permeable marly strata (Owen, 2003; Owen and Moretti, 2011). Laccolith-type injection structures associated with the lateral terminations of large load casts are thought to represent large-scale upward intrusions of fine sediments along open fissures (Owen et al., 2011). The large ball-and-pillow structures are interpreted

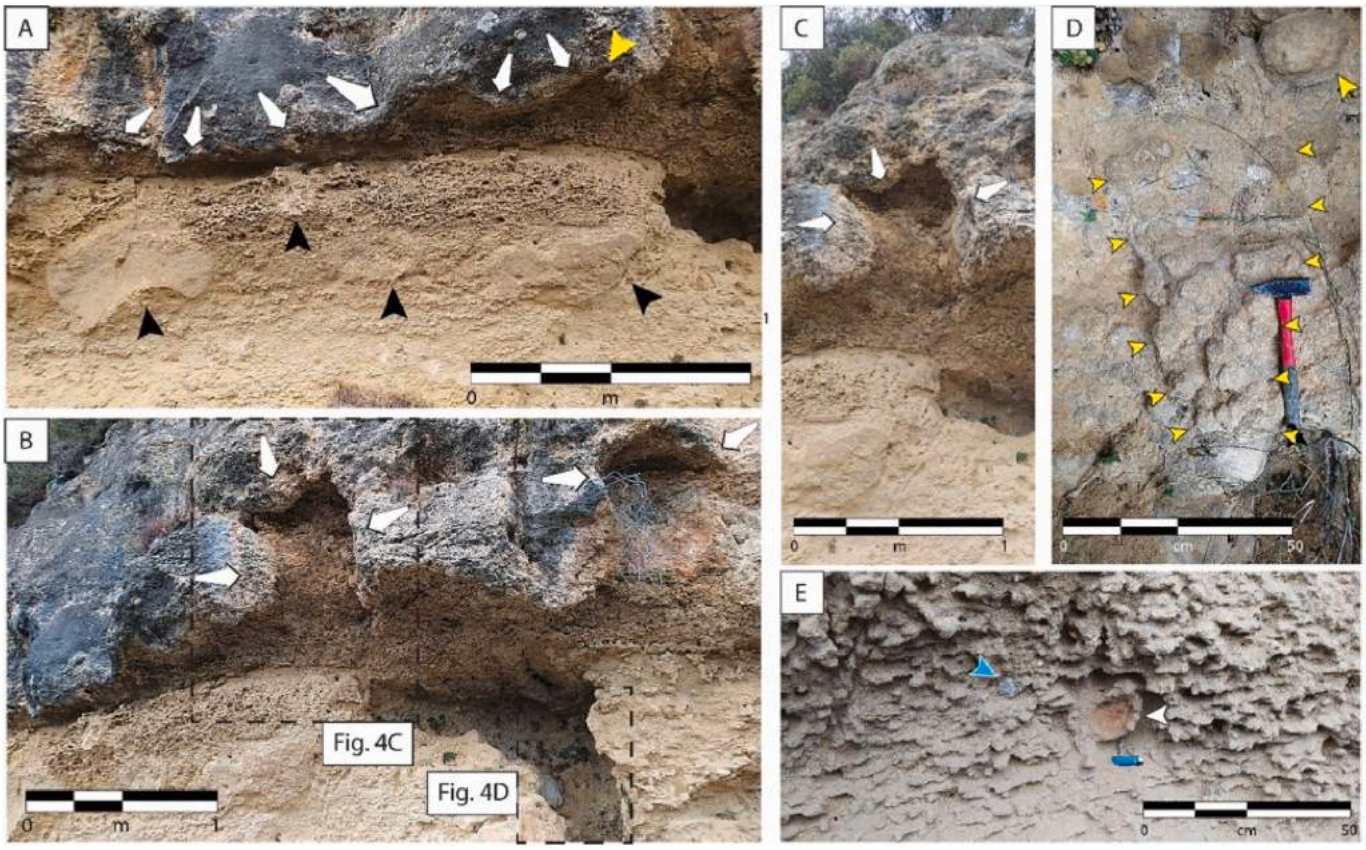

Fig. 4. A) Outcrop overview of the basal contact between conglomeratic layers and underlying marly sediments within the Perti Sandstones and Conglomerates member (Location 1; *Basal Complex of the Finale Ligure limestone Fm.*). See Fig. 4B for section locality. White arrows indicate load casts at the base of very thick conglomeratic bed. The marly interval features large-scale detached pseudo-nodules (black arrows) that float in a roughly parallel arrangement. B) Diapiric intrusions of marly sediments into fine-sandy strata of the Perti Sandstones Member. Rectangular inlet shows position of Fig. 4C&D. Also note the development of pseudo-nodules located at the lateral terminations of diapir-type intrusions (yellow arrow) C) Detail of laccolith-shaped injectite, displaying cusp tip morphologies at upper terminations. D) Close-up of area indicated in Fig. 4B, highlighting the downward-oriented, subvertical alignment of small-scale detached pseudonodules (small yellow arrows). E) Diagenetically overprinted foresets in sandy strata of the Perti member. Sediment dispersal was towards S-SW (160°). Note the isolated carbonate pseudonodule (white arrow) and the presence of conglomeratic clast (gneiss pebble highlighted by blue arrow) interpreted to reflect a relatively short transport distance from the adjacent Paleozoic basement of the Briançonnais domain.

to mirror density inversion resulting from the deposition of the thick sandy unit onto the finer grained marly interval. Their occurrence can be explained by the thickness of the marly layer and rapid deposition of the coarser grained strata that might have promoted the collapse of these ball-and-pillow structures into the underlying substrate (cf. Collinson et al., 2006).

The v-shaped clusters of small, attached well-rounded pseudonodules are however interpreted to result from the filling of meso-scale syn-sedimentary faults. These might have originated from sudden loading of the overlying sediments, presumably defined by uneven distribution of sediment load (Ricci-Lucchi, 1995; Ekwenye et al., 2020). The well-rounded shapes of the small pseudonodules are thought to be related to the impermeable nature of the surrounding sediments, bringing about cement precipitation and the development of concretionary nodules (Molenaar et al., 1988; Collinson et al., 2006). The single occurrence of an isolated small nodule is interpreted to have originated from disparate sorting of the sediments and by a contrasting proportion of carbonate cement with respect to the hosting sediments, presumably as a result of a carbonate fragment representing the nucleus of the nodule (Molenaar et al., 1988).

Notwithstanding the first-hand explanation of the triggering mechanism for liquefaction and/or fluidization that caused the SSDS would be that of rapid sedimentation that caused gravitational overloading onto the water-saturated fine-grained sediments (e.g., Owen et al., 2011; Ekwenye et al., 2020), an unambiguous deduction whether allogenic or autogenic drivers promoted the fluidization or liquefication of the SSD-prone strata is a challenging task. A range of indicators reasonably suggest an alternative explanation, namely a seismogenic trigger. Essentially the presence and the orientation of the laccolith-shaped structures indicates their occurrence in close association with open fissures (i.e. syn-depositional brittle faults as denoted in Fig. 4D; cf. Brandes and Winsemann, 2013; Van Loon and Pisarska-Jamroży, 2014). Moreover, the limitation of the SSDS to a single deformed stratigraphic interval of the investigated exposure, where lateral varieties of SSDS are observable (e.g., Moretti et al., 2014; Morsilli et al., 2020; Müller et al., 2021), together with the comparatively wide lateral extent of the SSDS-prone interval would provide further evidence of an earthquake-induced triggering mechanism responsible for the assemblage of SSDS recorded at study location 1 (e.g., Berra and Felletti, 2011; Moretti and Ronchi, 2011; Moretti et al., 2014).

4.2. Study location 2: boundary between the Basal Complex and PdF (Rocca di Perti)

Study location 2 (Rocca di Perti; Fig. 2) exposes the stratigraphic contact between the topmost 5–7 m thick "Perti conglomerates and sandstones" of the Basal complex (L6 of Della Porta et al., 2022) and the base of the "Rocce dell'Orera Mb." bioclastic limestones of the PdF (L11-12 of Della Porta et al., 2022). The boundary between the two units is defined by a sharp lithological contact, expressed by an abrupt grain

size jump from basal fine sandy sediments towards overlying coarse-grained bioclastic microconglomerates (Fig. 5). The fine sandy interval of the topmost "Perti conglomerate and sandstone" comprises massive sandstones that lack any evidence of primary sediment structures, whereas strata of the overlying "Rocce dell'Orera Member" typically show cross-stratification (Fig. 5C). Foresets dip towards S-SW. A detailed sedimentary facies analysis is documented by Brandano et al. (2015, 2022) and Della Porta et al. (2022). A variety of SSDS can be observed along the laterally continuous interface (see the 3D models as Link1-3; Link 1 - https://skfb.ly/oDAYw; Link 2 - https://skfb.ly/oDAYJ; Link 3 - https://skfb.ly/oDAZp). In the following a description of SSDS with primary focus on investigating differences in style, shape, and dimensions of the encountered structures is given (Fig. 5).

The most common types of SSDS are load casts and flames of variable morphologies that occur in a variety of dimensions. Remarkably, laterally crossing the interface along an SW-NE transect, a general trend in increase in dimensions and intensity of soft sediment deformation can be noted. While in many places the contact between the two units shows a straight to slightly wavy nature without direct evidence of disturbance except for minor loading (Fig. 5A), some zones in the NE' part display high abundance and diversity of SSDS. Based on disparate dimensions and morphological characteristics, three main types of load structures can be differentiated. At the smallest scale, an accumulation of load casts was encountered, associated with a sharp, irregular to wavy contact (Fig. 5B). These structures can be described as a continuous array of undulating load casts with dimensions of ca. 1–1.5 cm in height and 2–2.5 cm in width. The small-scale load casts generally display symmetric, concave-up profiles. They downwards intrude into the underlying fine sandy substrate. In some places, the small-scale variety occurs in association with larger counterparts. Medium-sized load casts are of symmetric, concave shape, with dimensions of ca. 20 cm in width and 10 cm in depth, exhibiting a half-circle (or lobate) shape in profile (Fig. 5C). Large-scale loading structures show maximum dimensions of ca. 1.70 m in width, with maximum downward extensions of ca. 1.40 m into the underlying substrate (Fig. 5D–E). In some places a transitional development from load casts into flame structures is observable (Fig. 5D).

Flame structures occur at different scales and display diverse shapes (Fig. 5E–I and Fig. 6A, B, E; see also the 3D models as Link1-3; Link 1 - https://skfb.ly/oDAYw; Link 2 - https://skfb.ly/oDAYJ; Link 3 - https://skfb.ly/oDAZp). Each type of flame structure is characterized by a sharp contact between the contrasting lithologies, defined by a pronounced grain size shift. These types of SSDS are characterized by upward-directed structures of fine sandy sediment into the overlying coarser-grained strata. Flame tips show a tendency to follow the orientation of the S-SW-directed main direction of paleocurrents (Fig. 5E). Both lateral and summit interfaces of the flame structures commonly display high-frequency wavy interfingered (Fig. 6D, F, G), or, in some places, cuspate-lobate morphologies (Fig. 6E). Flames are generally characterized by sharp, linear and angular lateral terminations (Fig. 5H; see also the 3D models as Link2; Link 2 - https://skfb.ly/oDAYJ).

At the larger scale, diapir-like structures that resemble mega-flames can be observed (5 F–I, 6 A-B; see also the 3D models as Link 1 and 3; Link 1 - https://skfb.ly/oDAYw; Link 3 - https://skfb.ly/oDAZp). The diapiric structures are up to 3 m in height and show sub-vertical orientations along the interface. They are limited to lateral terminations of the comparatively deep downward-directed intrusions of large-scale loading structures. Two main types of diapir-like shapes occur at study location 2. Diapir-like SSDS can generally be described as laterally restricted, curved protuberances that feature comparatively broad bases. In upward direction the diapiric intrusions show marked narrowing (Fig. 5E–G, 6A), and typically exhibit well-rounded to subrounded tops. In two cases slight kinks of the topmost part results in a "shark fin"-type of appearance (Fig. 5H). Above the top of large flames or diapirs, superimposing layers of bioclastic limestones are folded, accommodating the vertical shapes of the intrusions (Fig. 5F, see also Fig. 6A). Notably, concentrations of mud-clasts can be found at the immediate contact within the coarser grained "Rocce dell'Orera Member". Mud-clasts are arranged parallel to the top boundaries of large shark-fin like flame structures (Fig. 5E). In addition, several specimens of mega-flames can be observed. They are defined by sharp boundaries and angular flame shapes (Fig. 5H).

4.2.1. *Interpretation of SSDS*

Comparable to the suite of load-and-flame structures encountered at study location 1, their presence at the interface between the Basal Complex and the PdF (Rocca di Perti, location 2) is interpreted to result from liquefaction or fluidization of the lower stratigraphic interval (Moretti and Ronchi, 2011). Liquification or fluidization might either be triggered by the overpressure of the overlying sediment load (Moretti and Sabato, 2007; Van Loon, 2009), or by a seismic shock (Owen and Moretti, 2011; Van Loon and Pisarska-Jamroży, 2014; Van Loon et al., 2020). Overpressure is commonly regarded as a crucial prerequisite for the generation of clastic injectites (e.g., Van Loon, 2009; Rodrigues et al., 2009). Diapirs and megaflames thus suggest an origin in response to interstitial water overpressure, forcing injection of the underlying sediments into their overlying strata. Upward flow of liquefied sediments in the diapiric and flame structures is highlighted by several lines of evidences, including: i) the vertical alignment of the sands in the diapirs, particularly along the contact interface towards their hosting sediments, ii) deformation of sediments on their top and, iii) the interdigitated interface between sands and limestones and the cuspate-lobate features (Fig. 6G–E).

The sharp, linear and angular lateral terminations of diapir-like structures (Fig. 5 G&H) would imply brittle deformation in a somehow progressed state of lithification of the sediment. In comparison to overloading driven by high sedimentation rates that might account for the presence of load-and-flame structures, brittle deformation would therefore indicate an allogenic driver active after sedimentation (i.e. earthquake-induced seismic shocks; Van Loon and Pisarska-Jamroży, 2014), delineated by the fact that the liquefied body experienced conversion from solid-to liquid-state behavior (Berra and Felletti, 2011; Owen and Moretti, 2011). An increase in pore pressure might have promoted reduction of the tensional strength in the liquefied body in contrast with strengthening of the adjacent sediments, which resulted in geometrically sharp boundaries of the intruded fluidized sediments (Bryant and Miall, 2010).

4.3. *Study location 3: Verezzi member of PdF (Verezzi quarry)*

The studied outcrop at location 3 features a WSW-facing quarry-type cut of the calcarenitic "Verezzi Member" (Fig. 7; L10 of Della Porta et al., 2022). The quarry face shows lateral exposure of ca. 60 m and a cliff height of ca. 30 m (see the 3D model as Link4; Link 4 - https://skfb.ly/oDC6J). Since the quarry has only relatively recently been abandoned and has been exposed to the environment for less than 20 years, it does not exhibit evidence of strong weathering or alterations. The quarry face features at least three different disturbed intervals, distributed in different stratigraphic intervals (Fig. 7). The contact between comparatively homogeneous, coarse-grained calcarenites and superimposing finer, locally cemented and matrix sustained alternations of silty and fine sandy sediments can be studied (Fig. 8&9). The exposure displays evidence of a series of vertical water propagation systems that disturbed the original stratification of the sediments (Figs. 7 and 8). While the vertical outcropping exposure of the lowermost homogeneous coarse-grained calcarenitic strata is limited to ca. 2.5 m in height, the heterolithic finer-grained interval defined by alternating thin to very thin layers of mudstones and silts to fine sands accounts for the prominent wall (Fig. 7). In some places essentially the sediments involved in the interface are poorly consolidated. Parallel laminations are the common primary sediment structure expressed in the fine-grained alternations. Above the sharp contact between the two main facies, a

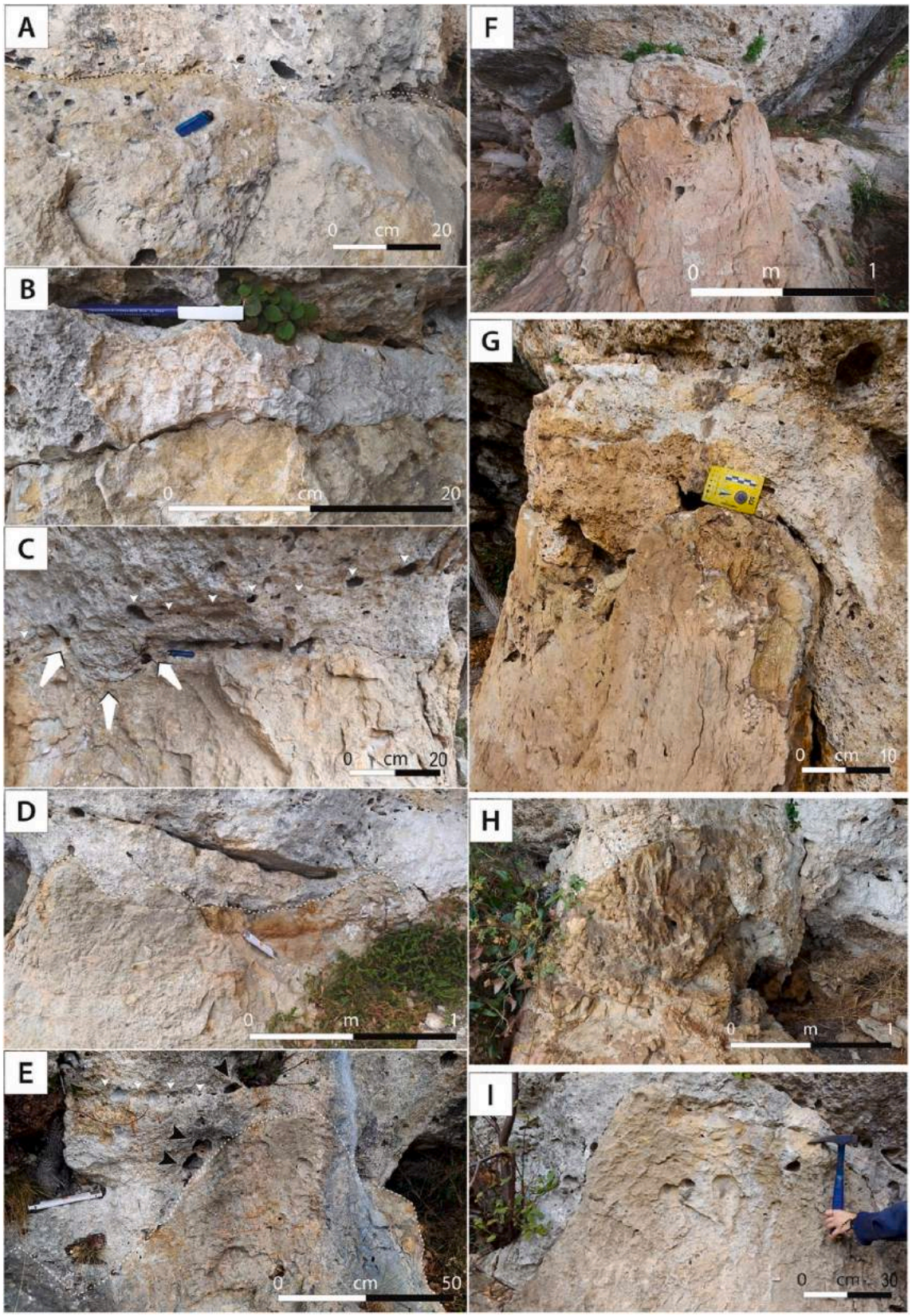

(caption on next page)

Fig. 5. Outcrop features at Rocca di Perti (Location 2), developed at the interface between the Torre di Bastia (*Basal Complex of the Finale Ligure limestone Fm.*) and the Rocce dell'Orera Mbs. (*Finale Ligure limestone Fm.*). A) Slightly wavy contact showing minor evidence of SSDs (isolated small-scale flame structures as indicated by arrows). Note the presence of mud-clasts in vicinity to flame structures. B) Small-scale symmetric load casts located at the base of undulating, wavy interface between the Rocca di Perti and Rocce dell'Orera Members. C) Medium-sized load casts found in association with alignment of mud-clasts in coarse-grained bioclastic strata. Note faint cross-bedding dipping to S-SW. D) Asymmetric concave-shaped large-scale load casts (white arrows) interpreted to indicate transitional development into flame structures E) Upward-intrusion of diapir-shaped flame structure into coarse-grained bioclastic strata. Note the abundance of mud-clasts in the intruded sediments (black arrows). F) Volcano-like structure defined defined by conical morphology. Note the above folded and sandwiched bioclastic strata. G) Detail of the summit of the structure in 5 F. Note the folded bioclastic limestones on the top of the diapir. H) Mega-flame structure that resembles shark fin morphology. Note the sharp-angular faulted lateral terminations of the diapir-like structure. I) Diapir-like structure defined by sharp-angular faulted lateral terminations and marked lithological contrast towards the superimposing sediments. To enhance the 3D perspective, see also the 3D models as Link1-3.

variety of SSDS can be observed. SSDS show disparate shapes and dimensions, and comprise (i) dome-shaped SSDs, (ii) intervals prone to load-and-flame structures, and (iii) chaotic and slumped strata. Their stratigraphic occurrence will be described in the following.

4.3.1. Dome-like structures

At the basal interface between the two lithologies, dome-like structures can be traced along the same stratigraphic level (Figs. 7A and 8; see the 3D model as Link4; Link 4 - https://skfb.ly/oDC6J). In terms of sediment grain size, the dome-like structures are characterized by comparatively homogeneous, medium to very coarse-grained sandstones, which intruded into their overlying heterolithic host rock that is predominantly made up of alternating siltstones and mudstones. In view of morphology, the structures range from dome-to oak tree-like shapes, with the latter typified by a central dyke-like vertical shaft that culminates in a fan-shaped crown (Fig. 8). Within a lateral distance of ca. 15 m, two well-preserved oak tree-like structures occur (specimen located the SW'part of the quarry is shown in Fig. 8A). Detailed investigation of the internal make-up of the tree-like structures reveals that the basal part of the structure is defined by a gradual contact with an undeformed layer. The core or shaft of the vertical structure shows a poor degree of cementation. Within the central dykes or in direct adjacency, intrusion carbonate filled veins and clastic dykes are observable. They vary from few mm's to ca. 1 cm in width, and can be distinguished by abrupt color changes (Fig. 10B, F), and show variable degrees of cementation. They branch into variably oriented channels that show a dendritic pattern, resulting in the tree-like morphology (Fig. 8A). A third dome-shaped SSDS can be observed in the southernmost part of the quarry (Fig. 8B). This structure is similar to the ones described above, although it lacks a central shaft. It should be noted that the main difference is that the injected sediments are coarser than those of the tree-shaped varieties, and that this southernmost dome-shaped SSDS is typified by a comparatively high degree of cementation. Moreover, it differs from the other dome structures as it lacks the lower undeformed layer, possibly due to limited exposure of the lowermost basal level in this part of the outcrop. The uppermost parts of all dome structures are represented by alternations of thin fine sandy and clayey layers, and feature assemblages of shear bands (Fig. 8B and 10C, E).

Granulometry analysis in the field via hand lens analysis reveals a rapid lateral and vertical shifts in grain size from coarse sandstones that represent undeformed strata below the domes and tree-like structures towards very thin alternations of fine laminated layers at their outer boundaries. Due to their in wide parts local unconsolidated state, sediments associated with the dome-like structure were additionally sampled for grain size analysis in the laboratory. Sample locations are indicated in Fig. 8B. Results from combined mechanical sieve and hydrometer analyses are shown in Fig. 9, confirming the sharp grain size contrast between the involved stratigraphic intervals. .

4.3.2. Chaotic strata with load cast SSDs

Within a vertical distance of ca. 11 m from the topmost part of the interval affected by the dome-shaped SSDS, a further deformed interval can be observed. The overall thickness of the affected stratigraphic interval is ca. 3.5 m (Fig. 7). Its basal part can be traced throughout the entire outcrop (see the 3D model as Link4; Link 4 - https://skfb.ly/oDC6J). Along a S–N transect, the thickness of the deformed interval shows a comparatively gradual decrease in thickness, with a northward reduction of the height of the deformation level which at its outer outcropping exposure is limited to ca. 50 cm. The features recorded in the layer comprise contorted/disturbed stratifications, upward sediment expulsions that cross-cut stratigraphic layers, and large loadings which are limited to the basal part of the disturbed interval (Fig. 7). On the neighboring quarry face the main SSDS features comprise load cast structures and mini-slump structures (from ca. 10 cm to 1 m in height). Towards the top of the quarry face another deformed interval can be observed. It shows similarity to the second deformation event; however, it is characterized by larger water intrusion features (Fig. 7C), which in turn up-section are followed by chaotically disturbed strata. Here, huge slump structures that resemble eye-shapes (Maino et al., 2015; 2021) occur in association with flames and fragments of incorporated strata (Fig. 7D–F). As for the previous deformation event, the vertical propagation changes between the two main analyzed walls of the cave.

4.3.3. Shear deformation bands and clastic dykelets

Arrays of deformation bands and clastic dykelets can be observed in both the Basal Complex and in the PdF. Millimeter-to centimeter-scale dykes are primary recognizable by marked color changes and/or protruding relief with respect to that of their hosting rock (Fig. 6C and 10B, F). Sedimentary clasts within the dykes range from sands to microconglomerate in size. Dykes are partially filled with carbonate cement, and may show alignments of spheroidal voids of mud eroded out of the sediments or lithic clasts (Fig. 10A). Post-diagenetic arrays of small fractures often retrace the dykelets' trajectories (Fig. 10A). Dykelets show sub-vertical arrangement, mainly striking NE-SW (Fig. 11B).

Deformation bands can readily be recognized by the offsetting of lamination sets; however they are difficult to detect in the more homogeneous sandy and calcareous layers (Figs. 8 and 10A, D-E). Band widths range from 0.1 mm to ca. 1 cm, with the latter being less frequent. Deformation bands displace sediment bedding planes from a few mm up to 2 cm (Fig. 10D–F). They often form conjugate networks or band arrays with dominant extensional kinematic and minor strike-slip component, and may thus classified as dilation shear bands (Fossen et al., 2007). Dome-shaped SSDS are dislocated by the shear bands, which in turn are offset by a second generation of flames (Fig. 8B and 10C-E). Dip angles range between 40° and 70°, showing well-defined NE-SW strike (Fig. 11). Field based comparisons of granulometric characteristics of shear bands and their hosting rocks reveal increased proportions of fine-grained sediments in the deformation bands.

Ten representative samples have been analyzed by petrographic investigation of thin sections. Two samples have been collected from undeformed sediments located in further distance from the deformation bands, four from either cement-rich horizontally oriented and cement-poor vertically oriented dykelets, two from shear bands and two from the basal coarse sands underlying the dome-like structure (Fig. 12).

Undeformed layers (Fig. 12A) are characterized by a dominantly muddy matrix (ca. 0.6 matrix/whole rock ratio). They show an average porosity of 4.4% and rare cemented areas. Modal composition is constituted by i) well-rounded lithic fragments of bioclasts, siltstones and dolostones and metamorphic grains (ca. 70%); ii) mono- and

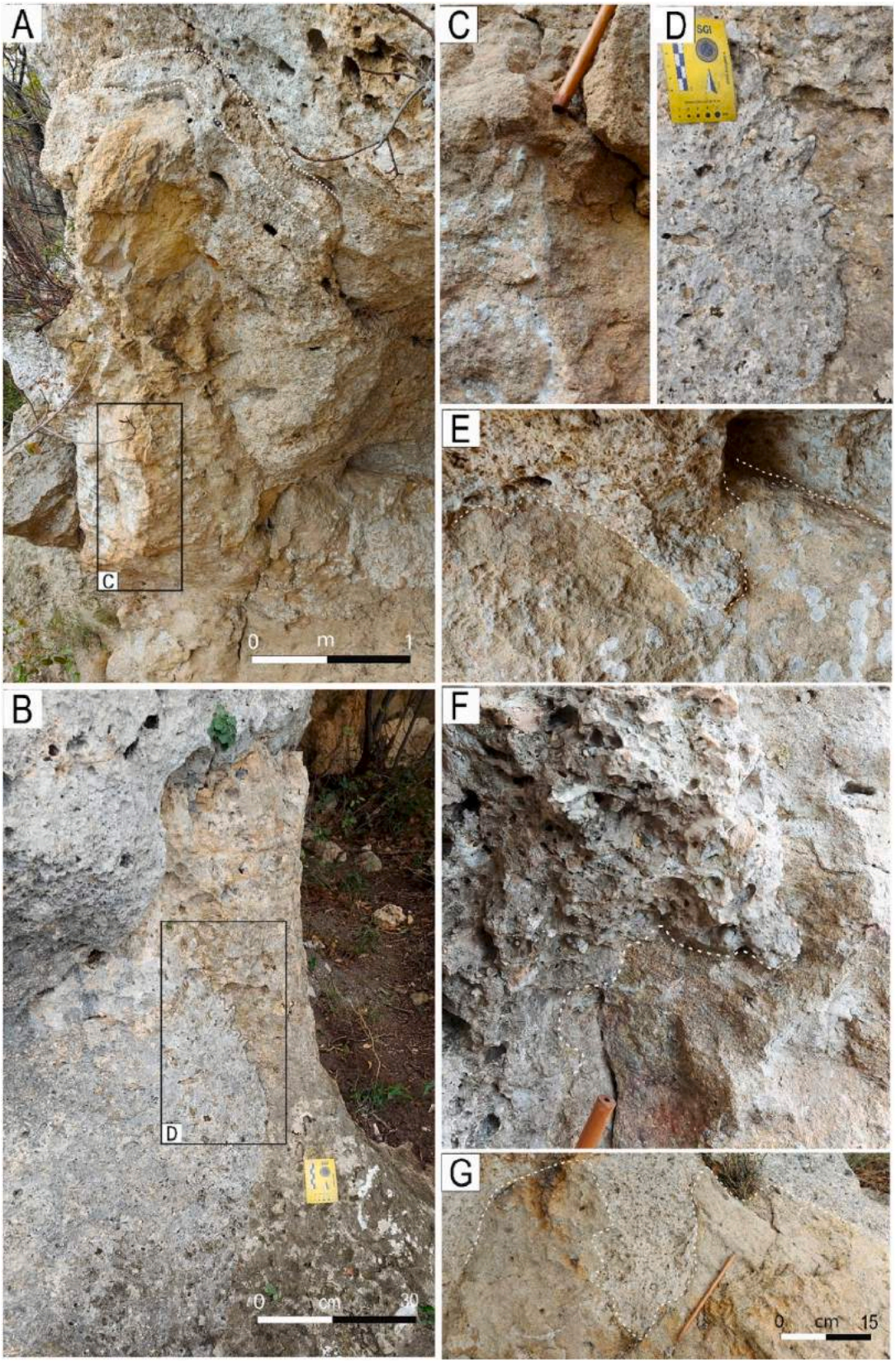

Fig. 6. Outcrop features at Rocca di Perti (Location 2), developed at the interface between the Torre di Bastia (*Basal Complex of the Finale Ligure limestone Fm.*) and the Rocce dell'Orera Mbs. (*Finale Ligure limestone Fm.*). A, B) Upward-intrusion of large scale diapir-shaped flame structure into coarse-grained bioclastic strata. Note the folded bioclastic limestones on the top of the flame in A. C) Detail of vertical sandy dykelet, highlighted by cemented vein in relief. D) Detail of the high-frequency wavy interfingered lateral interface of the flame structure in B). E-G) Cuspate-lobate morphology of flames that show alternations of sharp-angular and rounded boundaries. To enhance the 3D perspective, see also the 3D models as Link1-3.

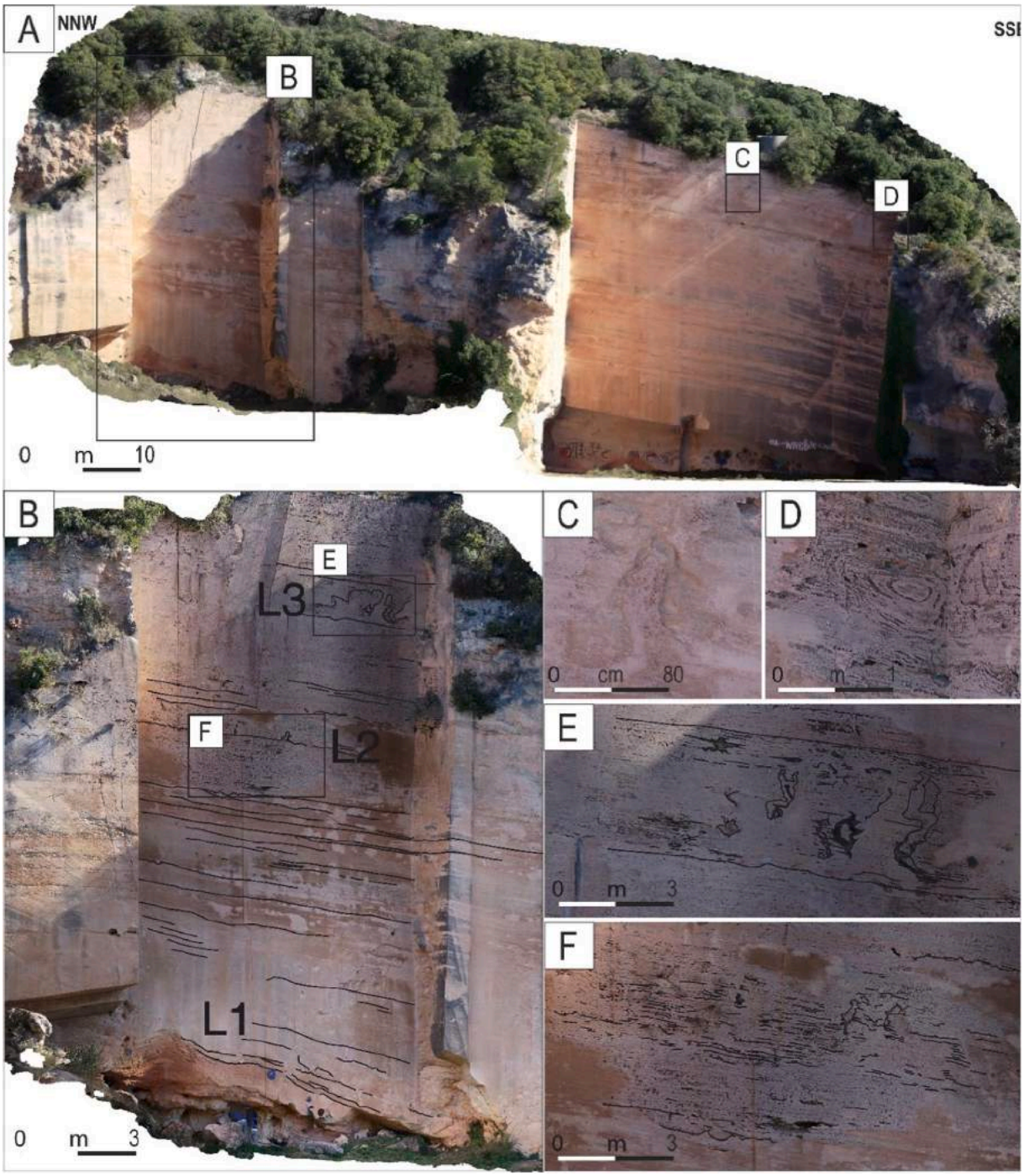

Fig. 7. A) Panoramic view of the quarry in the Verezzi Mb at the base of the *Finale Ligure Limestone Fm.* (Location 3). B) Stratigraphic distribution of SSDs recorded by three main layers (L1-3) within the Verezzi Mb. Structures of layer 1 are presented in Fig. 8. C) Detail of a worm-shaped vertical intrusion structure located in the topmost L3. D) Eye-shaped fold from the slumped and contorted layer 3. E, F) Details of chaotic structures including flames, fragments of incorporated strata and slumps. To enhance the 3D perspective, see the 3D model as Link4.

polycrystalline quartz with subangular shape (ca. 20%); and iii) micas and heavy minerals (ca. 10%).

The analyzed vertical dykelet from the main shaft of the tree-like structures (Fig. 8A) is a narrow (ca. 1 cm in width), matrix-rich (ca. 0.75 matrix/whole rock ratio) conduit that contains subangular to rounded clasts of lithic siltstones, micritic limestones, polycrystalline quartz and minor portions of volcanic fragments, mixed with mudclasts composed of host rock matrix (Fig. 12B). Clasts are arranged in moderate to strong alignments, essentially those with high aspect ratio (Fig. 12B). Within the dykelet carbonate cement is scarce, whereas it is more abundant in the adjacent rocks. Dykelet walls show vertically laminated thin (ca. 0.1–0.2 mm) layers made up of very fine material. Porosity in the dykelet is 2.9%, lower than that of the close host rock (4.7%), interpreted to reflect the relatively high proportion of mud matrix.

The dykelet sample collected from the low-dipping branches of the tree-shaped SSD (Fig. 12C) is richer in cement (cement to whole rock ratio of ca. 0.48). Cement is constituted by dolomite, calcite and ankerite, and contains clasts of lithic and mono-to polycrystalline quartz. It is characterized by a higher degree of sorting with respect to

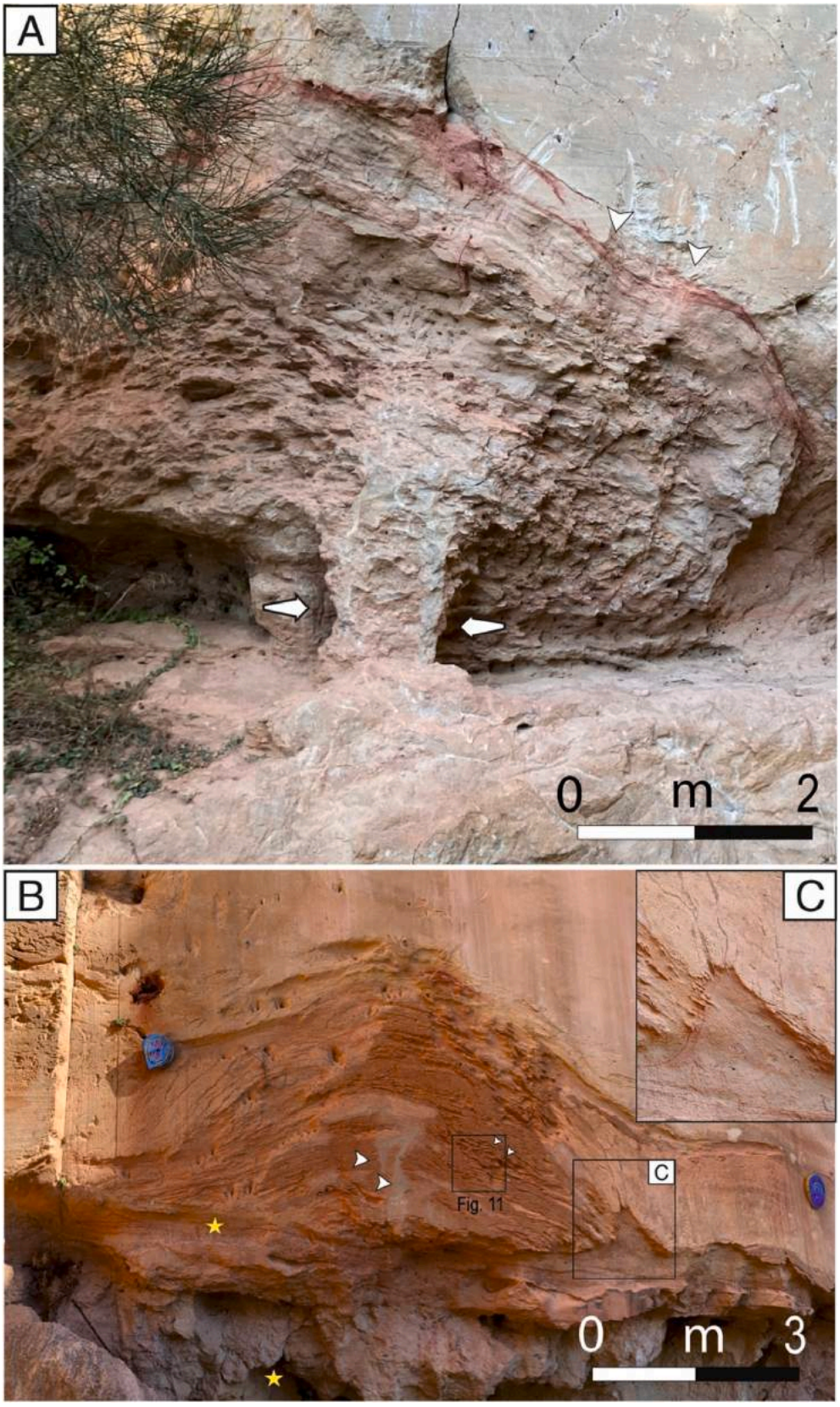

Fig. 8. Diapiric injectites distributed in the calcarentic Verezzi Member (Location 3). A) Giant oak tree-shaped intrusion defined by the central shaft that contains abundant sandy dykelets (large white arrows) and the fan-shaped morphology of the upper crown. Alternations of permeable and impermeable heterolithic strata characterize the topmost ca. 50 cm of the injectite, with the red-colored clayey layer marking the upper boundary of the crown towards its hosting sediments (small arrows). B) Dome-shaped upward-intrusion of coarse sandy sediment into superimposing thin-bedded heterolithic strata characterized by thin alternations of fine sand and clay. Note the shear bands cutting the dome (white arrows), and (inset C) a minor extrusion structure intersecting both the major dome and shear bands. Yellow stars indicate sample locations of unconsolidated sediments analyzed via mechanical sieving. To enhance the 3D perspective, see the 3D model as Link4. Small inlet indicates position of structural measurements of shear band orientations (see also Fig. 11C).

their surrounding rocks. Porosity is in the order of 1.6% in the cemented dykelet, while it makes up 5.0% in the host rocks.

Shear bands scattered within the heterolithic strata display laminated alternations of mud-rich and mud–poor intervals. They contain imbricated elongated clasts and show well-aligned orientations (Fig. 12D). Clasts are represented by well-sorted grains of quartz, feldspar, micas, and minor portions of sedimentary lithic fragments up to 2 mm in size. Mud-rich layers display more or less continuous alignments

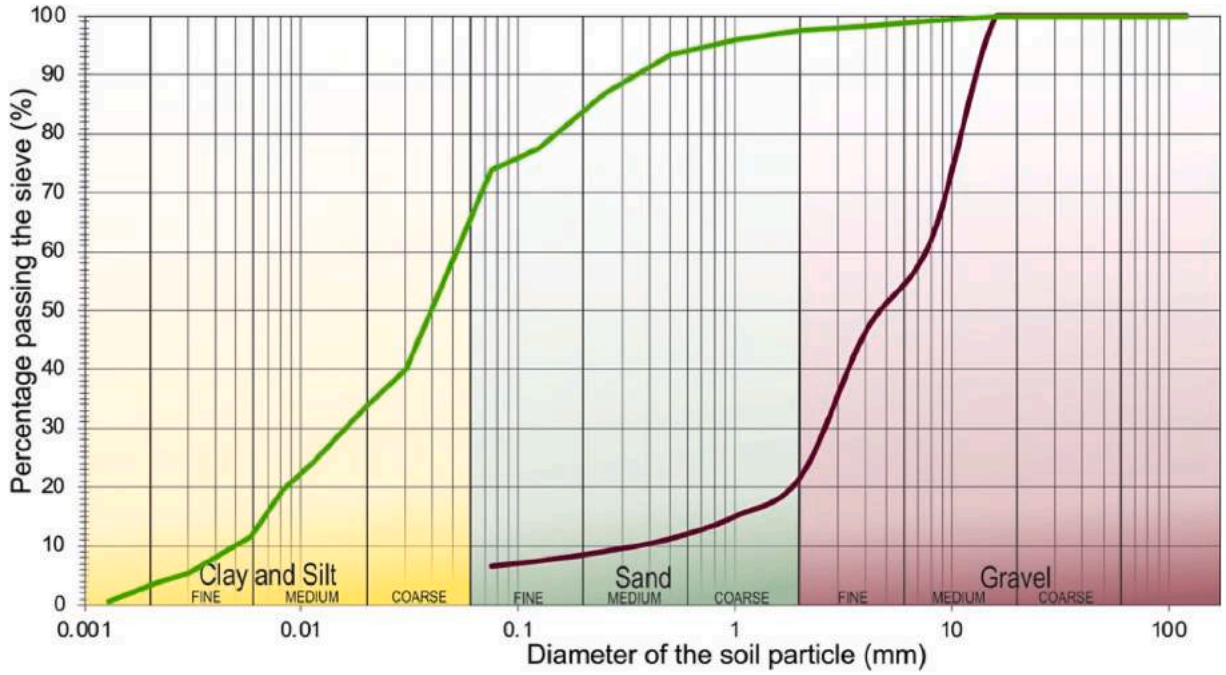

Fig. 9. Granulometry from mechanical sieving of strata (see Fig. 8B). Note the difference in content of clay-sized particles between the sample from the marly interval (green line) and the coarse sandy interval (magenta line).

of phyllosilicates, marking the visible foliation. Porosity of the shear bands is very low (0.4–0.8 in the fine, and 0.3–0.7 and coarse layers).

Sandstones and conglomerates below the big dome-like structure are characterized by a marked increase in grain size (Fig. 12E). Calcarenites consist of large clasts of limestone, lithic fragments and mono-to poly-crystalline quartz, characterized by minor alignment. Carbonate cement and mud matrix fill gaps among clasts with a cement&matrix to whole rock ratio of ca. 0.12). Calculated porosity of these coarse sandstones is of 5.0%.

4.3.4. *Interpretation of the SSDs*

In the basal part of the studied exposure the PdF exhibits remarkably large (up to 5 m in height) specimen of dome- or tree-shaped SSDS which provide compelling evidence of upward-directed escape of highly pressurized fluid-sediment mixtures into their hosting strata (Rodríguez-Pascua et al., 2000; see Fig. 13C). The stratigraphic layer prone to liquification in this case is represented by coarse-sands, which are capped by alternations of sandy and silty layers, stratigraphically set in the lower part of the Verezzi member (L10 of Della Porta et al., 2022). Up-section, the recurrent presence of slumped strata, large contorted intervals that resemble eye-shaped structures and mega flames is regarded to denote the cyclic nature of deformational events (e.g., Rodríguez-Pascua et al., 2000; Ettensohn et al., 2011; Müller et al., 2021). Given the relatively horizontal style of bedding and the comparatively mud-poor nature of the sediments, a depositional origin of the slumped intervals that would require comparatively steep slopes (Martinsen, 1989) can feasibly be ruled out. In low-angle slopes, liquefaction promoted by the drastic reduction of the shear strength results in a plastic behavior of the sediments. We favor the interpretation of a seismogenic origin of slumps, which has widely been documented elsewhere (e.g., Dead Sea Basin; Alsop et al., 2016). Here the stratigraphic repetitions of slumped intervals could reflect aftershocks of the same seismic event (Rodríguez-Pascua et al., 2000).

4.4. *Shear deformation bands and clastic dykes*

A key argument for the disclosure of the relationship between SSDS and their trigger mechanisms is the abundance of deformation bands that may be associated with regional tectonic structures (Brandes and Tanner, 2012; Brandes et al., 2018a, 2022; Mueller et al., 2020). We document several non-cataclastic shear deformation bands that display dominant normal offset and minor strike-slip, and may thus classified as dilational shear bands (Fossen et al., 2007). Moreover, depending on the phyllosilicate content they can be further classified as disaggregation or phyllosilicate bands (Fossen et al., 2007). The low percentage of crushed grains and angular and/or fractured clasts favor a granular flow deformation mechanism, where motion of grains was dominated by intergranular rotation and sliding (Twiss and Moores, 1992). Similarity in grain-size between the shear bands and their surrounding rocks suggest the absence of significantly reduced grain size of the disaggregation bands, thus excluding dominant cataclastic processes. Shear bands are accompanied by nearly vertical matrix to cement-rich dykelets, derived from intrusions of fluidized sands in relatively more competent sediments (Figs. 6–8, 10). Big extrusion structures (domes, tree, flames) are fed by dykelets and shear bands. The fact that they are dislocated by shear bands and, in turn, by other minor fluid escape structures (Fig. 8B and C), demonstrates an evolution marked by multiple episodes of deformation, in part related to fluid injections. Collectively, the arrays of shear bands and dykelets have been documented in a spatial extent of more than 10 km^2 in both the Basal Complex and PdF formations. They display a constant and common NE-SW strike (Fig. 11), which matches that of post-collisional regional faults mapped along the Ligurian margin both onshore and offshore (Fig. 2B; Boni et al., 1971; Vanossi et al., 1986; Morelli et al., 2022).

Grain orientations and alignments of elongated grains increase from outward to inward positions within the band and dykelet, a trend that inversely correlates with porosity (Fig. 12). Pore-space reduction may be the result of i) denser grain packing, and/or ii) cement-matrix enrichment. Realignment of particles is typically promoted by shear (Wegner et al., 2014). However, also post-deformation cement precipitation played a significant role in porosity reduction. In this case, a syn-shearing transient increase in porosity and permeability can be inferred, as described in many experiments (e.g. Main et al., 2000). Shear bands commonly result in channelization of fluids, thus promoting dissolution and precipitation processes. The more abundant cement content in the low-angle dykelets in comparison to the vertical ones

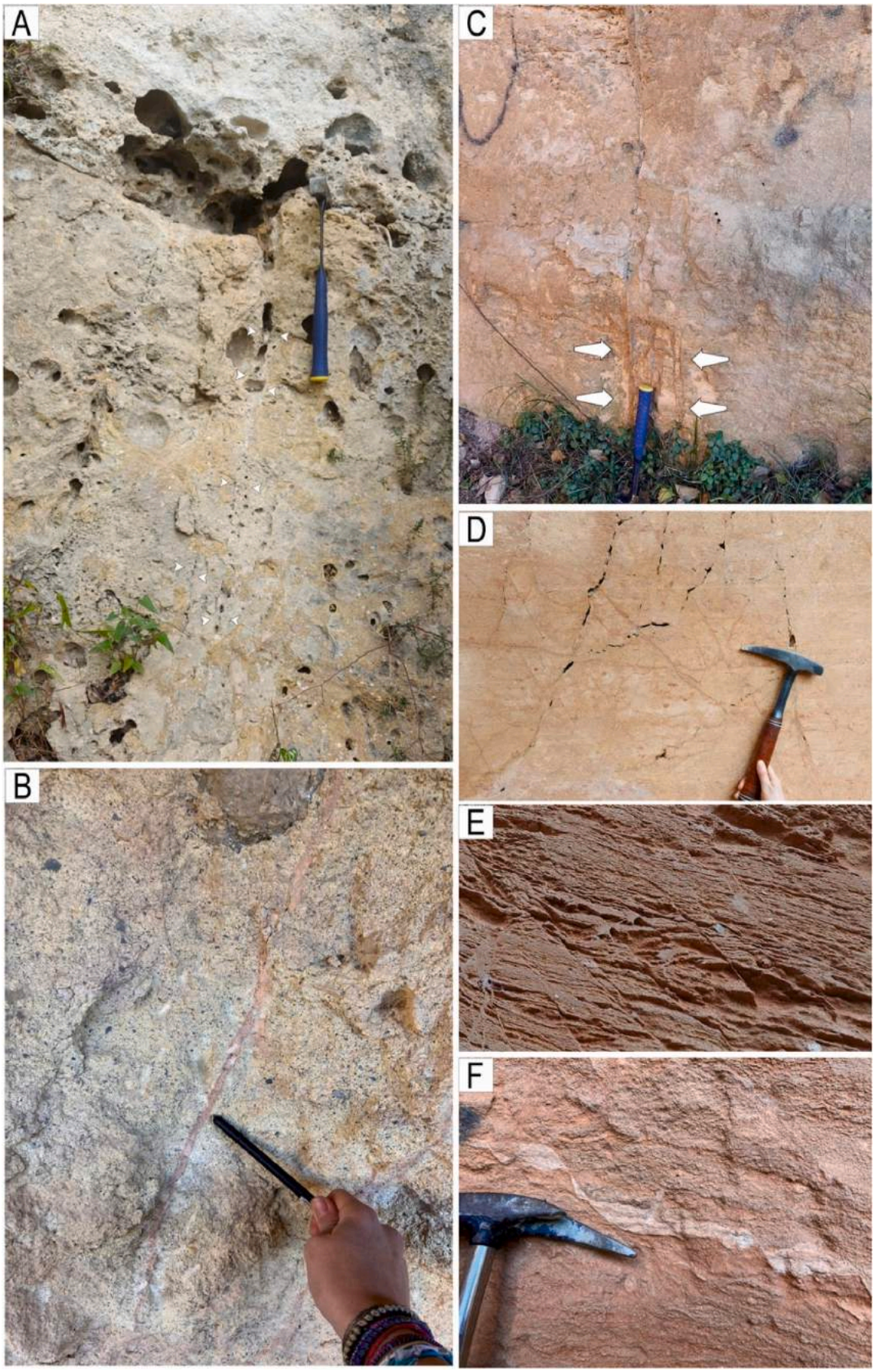

(caption on next page)

Fig. 10. Deformation structures from Location 2 and 3. A) Clastic dykes partially filled with carbonate cement, highlighted by alignments of spheroidal voids of mud and post-diagenetic fractures. B) Reddish strait chimney of fine grained material crosscut the sandy layers at the base of the dome-shaped structure of Fig. 8B. C) Sub-vertical clastic dikes are highlighted by protruding relief with respect the host rocks (Verezzi Mb of PdF). D-F) Shear bands characterized by mm-to cm-scale of dominant extensional displacement. D) Conjugate shear bands in the Verezzi Mb, right to the dome-structure of Fig. 8B. E) Set of shear bands displacing the laminations of the large dome-shaped structure of Fig. 8B (see Fig. 8B for the location). F) A relatively cement-rich layer displaced by shear bands in the Verezzi Mb., located to the right of the large tree-like structure of Fig. 8A.

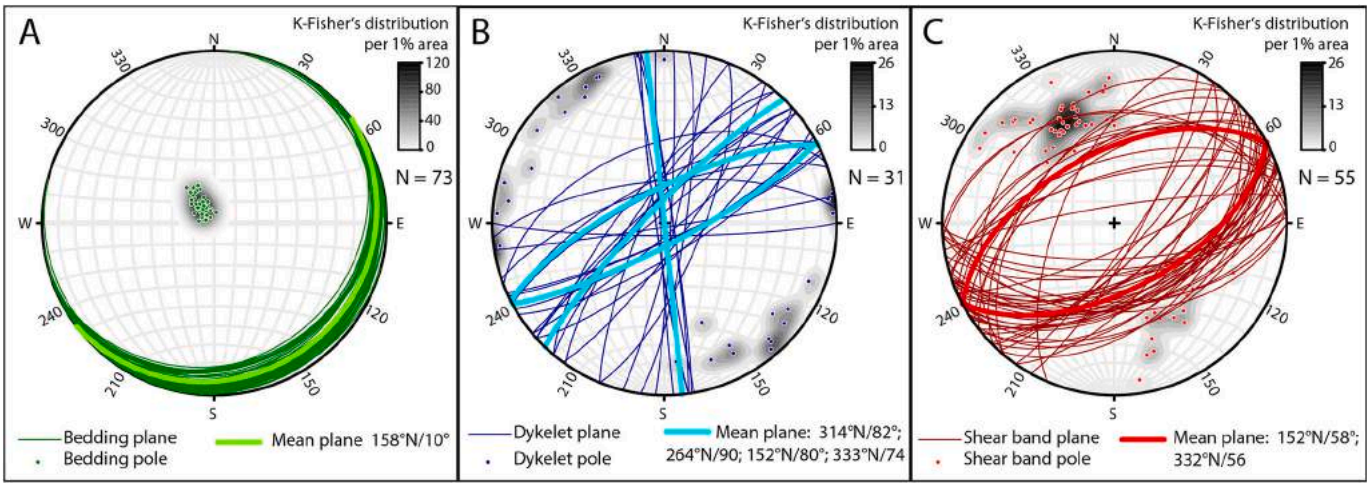

Fig. 11. Stereogram (equal-area, lower-hemisphere projection) of bedding (A), dykelets (B) and shear bands (C) measured in Locations 2 and 3.

(Fig. 12 B, C) further suggests rapid and transient transition of fluids into the central shaft of the tree structure, with fluid flow stagnating in the upper branches.

Overall, shear bands and dykelets described at the Basal Complex – PdF interface provide strong evidence of syn-deformational upward fluid injection due to excess in pore pressure. Liquefaction of water-saturated sands and consequent groundwater expulsion requires a high strain rate, thus supporting the argument of a seismic trigger (e.g. Moretti and Owen, 2011). Based on the age of the Verezzi Mb., seismic activity could hence be constrained to have occurred in Langhian-Serravallian times.

5. Discussion

The Finale Ligure Basin preserves a suite of SSDS that range from small size (<1 m) load casts, mini-slumps, flame structures (Fig. 13A) and pseudonodules to large-scale (several meters) slumps, chaotic strata, sand intrusions and diapir- and tree-like injection structures (Fig. 13B). All SSDS developed throughout the stratigraphy are related to interfaces marked by strong lithological contrasts in terms of both granulometry and sedimentary facies. Differences in style and dimension of the investigated SSDS are interpreted to reflect disparity in both the mechanisms that formed the intruded sediments, and in facies and texture/composition of their parent deposits.

5.1. Deformation mechanisms

The relatively small (cm-scale to <1 m) deformations recorded along the interface between marly and sandy to conglomeratic layers (Location 1) are interpreted to result from gravitational loading (Fig. 13A). Load structures represent a form of SSDS that - with respect to the deformed bedding surface - either show downward-orientations as typified by load casts and pseudonodules, or follow upward trajectories as expressed in flame structures and diapirs (Owen, 2003; Owen and Moretti, 2008; Oliveira et al., 2009). The most common load casts presumably originated from rapid deposition of high-density sandy sediment over its underlying less dense marly substrate. This is interpreted to have resulted in gravitational instabilities caused by a reversed density gradient (e.g., Moretti and Sabato, 2007; Owen et al., 2011). Flame structures are thought to have formed as upward-directed hydroplastic intrusions of marly substrate into the loading structures (Oliveira et al., 2009; cf. Lowe, 1975). The pseudonodules distributed in the marly horizon may therefore likely result from sediment loading and detachment of the denser sand into the less dense underlying shale interval (Owen, 2003; Owen and Moretti, 2008; cf. Ekwenye et al., 2020).

By contrast, SSDS from Locations 2 and 3 display evidences of intrusions of fluidized sands (Fig. 13B). Water-escape structures here developed at contrasting lithological interfaces represented by the transition from i) relatively fine sands to coarse-grained bioclastic sands and microconglomerates (Location 2) or ii) coarse sands to silty-rich layers (Locations 3). Vertical conduits, up to 5 m in height resembling diapir, dome- or tree-shaped morphology, emphasize the larger-scale deformations (meter to tens of meters in size). Such structures witness overpressurized water-injection, due to liquefaction and fluidization of the underlying sandy beds, which are capped by low-permeability marly layers (as in Location 3). Here, this clayey level provides a permeability barrier that generated a water confinement in the sandy volume below (Fig. 12C). Either way, the low-viscosity mix of water and sediments moved upward, cutting the low-permeability cap (as expressed in dykelets and veins) and deformed the overlying sediments (e.g. Owen, 1987). Adjacent materials behaved in a plastic or brittle way, giving rise to folding (slumps, cuspate-lobate structures, and smoothed flames) or brittle rupture (flames defined by angular shapes and shear bands). Liquefaction represents the better explanation as it would furthermore account for the formation of slumps and chaotic strata (Location 3) along a comparatively flat slope.

5.2. Driving forces

In general, SSDS can either be the result of internal controls directly related to given conditions of the depositional environments (i.e., rapid sedimentation, density contrasts, reworking of sediments by mass movement or wave action), or they can be induced by external triggers such as seismic shocks or impact events (Owen and Moretti, 2011; Shanmugam, 2017). SSDS recorded in the Finale Ligure Basin are related to i) gravitational instabilities and ii) fluidized injections of liquefied

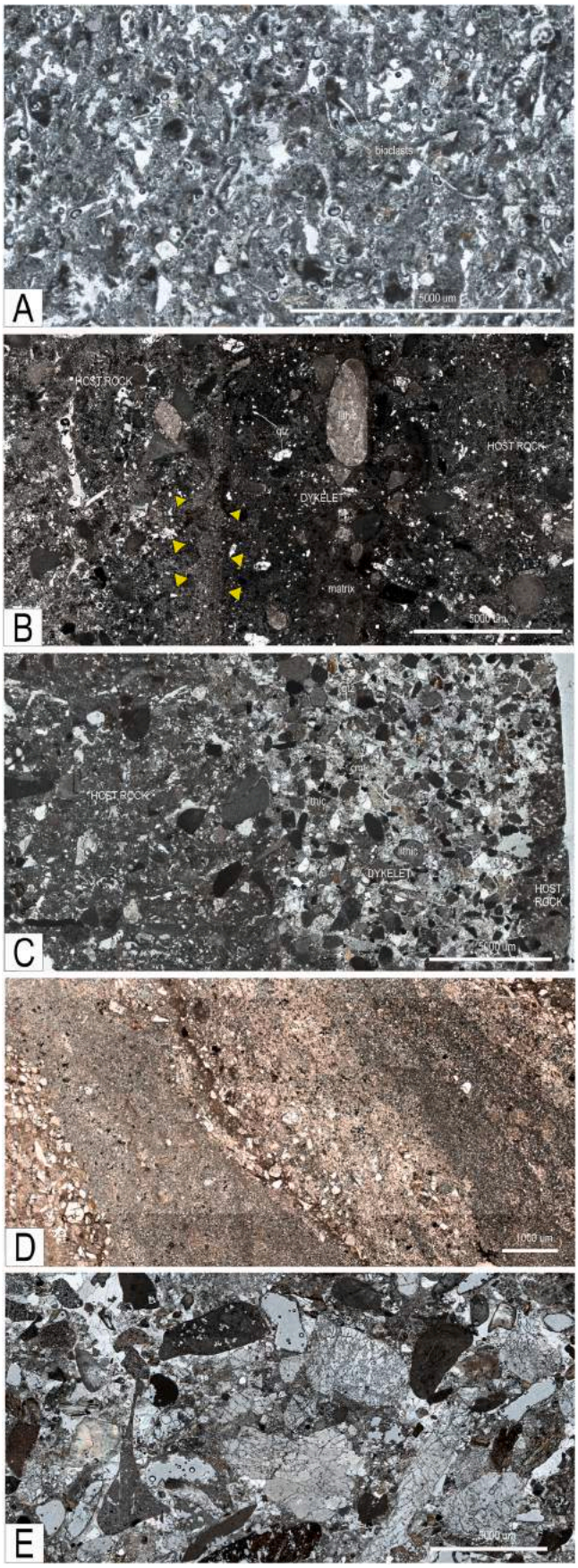

(caption on next column)

Fig. 12. Microphotographs (polarized light) of representative samples. A) undeformed bioclastic sands consisting of a muddy matrix encompassing mono- and polycrystalline quartz and micas, lithic fragments of bioclasts, siltstones and dolostones and metamorphic grains. B) Vertical, mud-rich dykelet containing moderately to strong aligned clasts of lithic siltstones, micritic limestones, polycrystalline quartz, volcanic fragments and mudclasts. Note the imbrication of large high-aspect clast. Carbonate cement is enriched in the domains adjacent to the dyke. Yellow arrows highlight vertically laminated thin walls of very fine material bounding the dyke. C) Cement-rich low-dipping dykelet including lithic fragments and mono-to polycrystalline quartz grains. Surrounding host rocks show high content of muddy matrix. D) Shear bands displacing the dome structure display alternate mud-rich and –poor laminations that contain imbricated and well-aligned clasts of quartz, feldspar, micas, and lithic fragments. Mud-rich layers are dominated by phyllosilicates. Shear bands are characterized by absence of evidence of cataclastic process and may be classified, based on the mica content, as disaggregation to phyllosilicate shear bands (cf. Fossen et al., 2007). E) The basal homogeneous, coarse-grained calcarenites representing the lower unit sourced from the dykes and fluidized upward in the dome-like structure. Note the strong depletion of fine-grained material.

sands.

Loading structures commonly originate when dense sediments settled into less dense, highly water-saturated fine-grained strata below (e.g. Owen, 2003; Moretti and Sabato, 2007; Van Loon, 2009; Owen et al., 2011). A non-uniform sediment density gradient and dissimilar loading of the overlying deposits can generate driving forces that act synchronously with liquefaction/fluidization processes. Therefore, the two processes (gravitational instabilities and liquefaction) may act simultaneously. Additional triggering mechanisms to that of a reverse density contrasts can be represented by rapid sedimentation or storm events (cf. Ekwenye et al., 2020). Notwithstanding, exogenic triggers for the development of load-and-flame structures such as seismic shocks has to be considered. The development of syn-sedimentary folds can alternatively be explained by the brittle nature of the cohesive marly substrate, assuming that excess pore water pressure was too low to induce liquefaction of the fine-grained sediments (cf. Rossetti and Góes, 2000).

Liquefaction and/or fluidization processes can alternatively be generated during several natural processes, and the recognition of the trigger(s) remains difficult. Following the criteria commonly used to interpret the trigger mechanisms (e.g. Moretti, 2000; Owen and Moretti, 2011; Moretti et al., 2014), we hereafter discuss three possible agents leading the formation of the SSDS in the Finale Ligure Basin, including: i) rapid sedimentation, ii) wave-induced overloading, or, iii) seismicity.

5.2.1. *Rapid sedimentation*

Given the abundance of loading structures, an interpretation that favors rapid sedimentation causing gravitational instability and promoting a reverse density gradient and liquefaction and subsequent development of SSDS needs to be considered (Allen, 1982; Mills, 1983; Owen, 2003; Owen et al., 2011; Ekwenye et al., 2020). Generally, the tidally- or wave-influenced, a comparatively proximal deltaic system environmental interpretation for the Finale Ligure Basin, would favor the development of SSDS triggered by slope instability, storm waves, and/or overloading associated with high-flow discharge (e.g. Bann and Fielding, 2004; Oliveira et al., 2009; Owen et al., 2011). Nonetheless, the nearly flat slope depicted by the PdF and its Basal Complex strata allows to easily rule out this mechanism as generating slumping. Rapid deposition of vast amounts of sediments on water-saturated sands is an efficient mechanism that might promote liquefaction in the underlying sandy layer (Owen et al., 2011). The cross-bedded sandstones - locally capped by marly layers - are ideal candidates to develop liquefaction (Kolbuszewski et al., 1950; 1953). Most liquefaction originates in sediments buried less than 5 m up to a maximum of 10 m in depositional depth (Crespellani et al., 1988; Obermeier, 1996; Owen et al., 2011). Considering the huge dimension of diapirs (up to 3 m high) and dome- or tree-like structures (up to 5 m in height), complete liquefaction of the

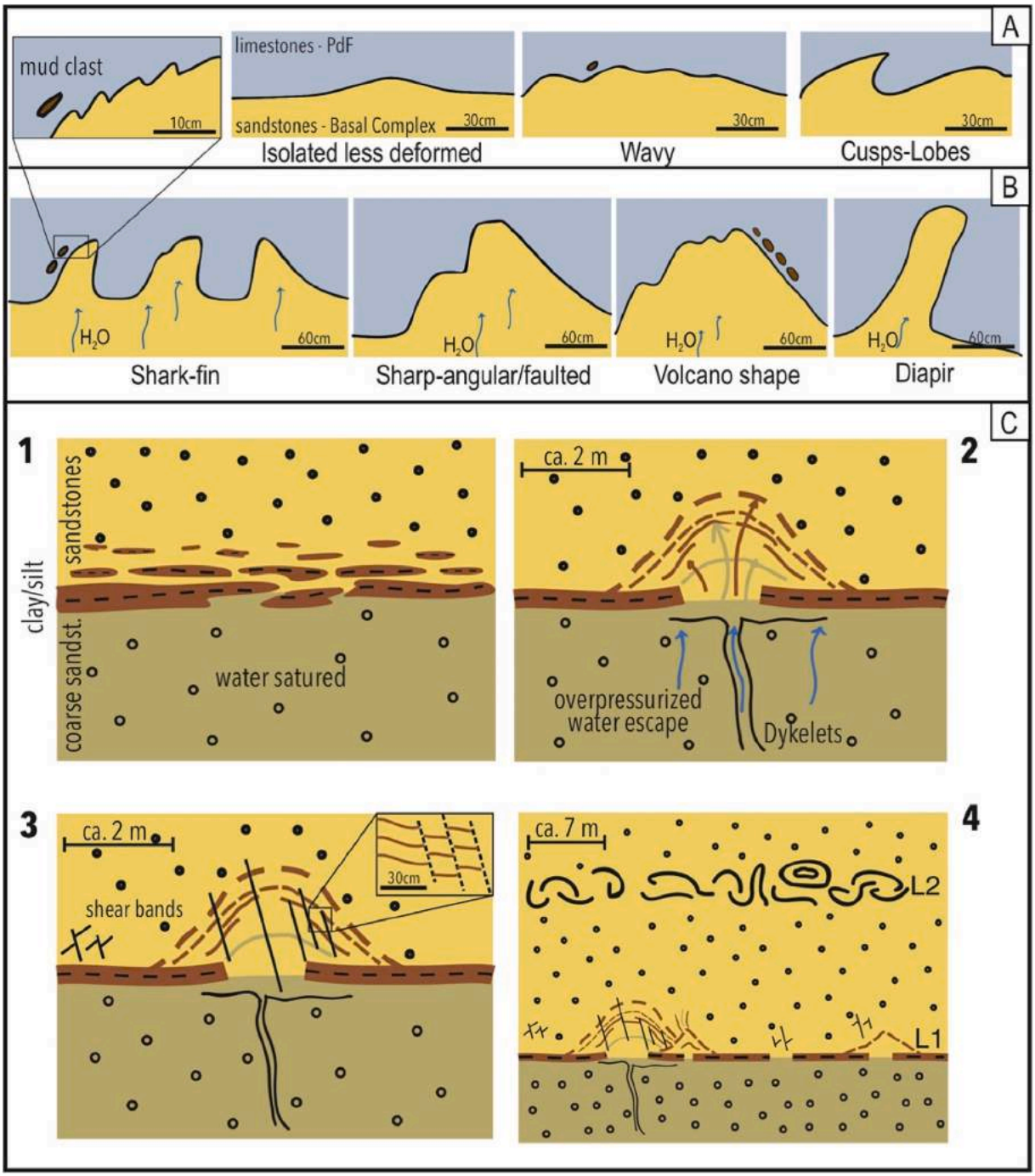

Fig. 13. A-B) Cartoon summarizing the main features of observed SSDS. A) small-size (<1 m) load casts, slumps, flame and pseudonodules, interpreted as resulting from overloading caused by reversed density gradient. B) Morphology of the larger-scale (>1 m) flames and diapirs. C) Attempt of a conceptual model for the formation of the giant water escape dome morphology and the associated shear deformation bands. Cartoon 1 describes the pre-deformation state of the coarse sands of the Basal Complex below and the relatively finer calcareous sands of the Verezzi Mb. Of the PdF above. The margin of the injectite is represented by discontinuous marly layers. 2) Transient seismic shock-induced liquefaction of the water-satured lower layer capped by marly level. Water is channelized within sandy dykelets and ejected into the upper layers, producing the dome-shaped morphology. 3) Disaggregation and phyllosilicate shear bands crosscut the dome structures. They may have developed in response to both earthquake and slow creeping (Brandes et al., 2022), and may thus potentially indicate the seismic and aseismic movement. 4) Further seismic deformation is highlighted by new water extrusion (see Fig. 8C) and diapiric sand intrusions crosscutting the earlier dome and disaggregation bands, while up-section slumps and chaotic disruptment of strata develop.

underlying sandy layer (5–7 m) would require the sudden arrival of a mass of ca. 4–10 m thick sands (depending on the presence of a low-permeability cap of the underlying the layer; cf. Moretti et al., 2001). Nearly instantaneous deposition of such thick sediments may occur during huge mass transport deposits, which are commonly represented by slumps, slides and debris flows. As no evidence of huge mass transport deposits is recorded throughout the entire Finale Ligure Basin, an alternative solution invoking seismically-triggered liquefaction needs to be considered.

5.2.2. *Storm wave-induced overloading*

In view of recent updated interpretations of the depositional

environment of the PdF that suggest a high-energy scenario (Brandano et al., 2022; Della Porta et al., 2022), a wave-induced explanation of SSDS should equally be considered as the trigger for SSDS in the Verezzi Member of the PdF (Location 3). Tempestites as the driving mechanism for SSDS have been considered elsewhere (e.g. Molina et al., 1998). Notwithstanding, the lack of documentation of other primary sedimentary structures indicative of wave activity below the fair-weather wave base such as hummocky cross-stratification might somehow argue against the interpretation of a high-energy wave-dominated depositional environment (cf. Della Porta et al., 2022). A further indicator that would argue against a wave-induced driving mechanism is the frequent orientation of flame tips in down-current direction. Following the early interpretations of a tidally influenced, shallow-water delta, we interpret the presence of bi-directional laminations and the common presence of trough cross-bedding (Boni et al., 1965) as rather indicative of a depositional environment above the storm-weather wave-base (Collinson et al., 2006; see also Peters and Loss, 2012). Based on ichnological observations, Baucon et al. (2020) propose a high-energy setting defined by high sedimentation rates and the presence of wave-like bedforms. The presence of mud-draped cross-beds (Boni et al., 1965) would here however rather point towards an estuarine to transitional marine environment subjected to tidal currents. Moreover, Della Porta et al. (2022) propose that the Verezzi member was deposited in the more distal part of the interval in water depths ranging from ca. 7–70 m of depth, thus, likely at depth greater than 30 m. Wave-induced liquefaction instead typically occurs at depths between 10 and 20 m (Okusa, 1985; Alfaro et al., 2002). Enormous waves (associated with tsunami) are required to generate water-escape structures up to 5 m in height. Given the vast dimensions of clastic injectites and their juxtaposition with minor load-and-flames and shear deformation bands we tend to rule out a wave-induced triggering agent for the observed SSDS.

5.2.3. Seismicity

At first consideration, the analyzed structures show similarity in morphology with several SSDS associated with earthquakes (e.g., Allen, 1982; Afaro et al., 1997; Moretti and Sabato, 2007; Moretti and Ronchi, 2011; Owen et al., 2011; Mugnier et al., 2011; Rodríguez-Pascua et al., 2000; Rudersdorf et al., 2015; Hilbert-Wolf et al., 2016; Brogi et al., 2018; Fattah and Abu Sharib, 2023). Large-scale (>1 m) load-structures and water-escape structures (flames, diapirs, tree-like structures) are commonly interpreted as seismites (Seilacher, 1969; Obermeier, 1996; Moretti and Sabato, 2007; Alfaro et al., 2002; Mugnier et al., 2011). Slumped and contorted intervals can equally be interpreted as triggered by earthquakes, essentially as they are distributed in basinal environments characterized by low slope gradient (e.g. Bhattacharya and Bandyopadhyay, 1998; Rodríguez-Pascua et al., 2000; Mugnier et al., 2011; Liesa et al., 2016; Alsop et al., 2016; Vitale, 2018). Sediment grain size indicates that the coarse to fine sands involved in the fluidized process meet the requirements to activate liquefaction processes due to earthquakes (e.g., Allen, 1982; Galli, 2000; Montenat et al., 2007; Owen and Moretti, 2011; Caputo et al., 2016). The large spatial extension of SSDS within an area that covers more than 10 km^2, their lateral continuity and the vertical repetition of deformed horizons interpreted as mobilized by seismically induced liquefaction (Fig. 7) are further criteria consistent with a seismic trigger (Owen and Moretti, 2011; Müller et al., 2021).

Seismically-induced liquefaction requires the proximity of SSDS to one or more faults likely to have been active during sedimentation. In the study area, evidences of fault activity during the Miocene are lacking, but new mapping revealed the presence of arrays of dilatational disaggregation bands in both the Basal complex and Pdf sandstones (Fig. 10). They show constant NE-SW striking, matching the main structures in the underlying basement (Fig. 1B). Shear deformation bands show dominant extensional kinematics and complex interaction with water-escape structures, suggesting multiple deformation episodes (Belzyt et al., 2021). Shear bands are associated with vertical carbonate-filled veins and dykelets, and are exposed throughout the mapped area. They acted as preferential conduits during co-seismically groundwater-expulsion (e.g. Scholz and Frieling, 2006; Hargitai and Levi, 2014). The lateral and vertical extension of shear bands with a constant strike is the key criterion to distinguish fault-related disaggregation bands from those resulting from non-tectonic processes (Fossen et al., 2010; Brandes et al., 2018a, 2022). Recent studies show that shear deformation bands formed near surface in unconsolidated sediments can serve as a reliable indicator for the activity of faults in the underlying basement (Cashman et al., 2007; Brandes and Tanner, 2012; Brandes et al., 2018a&b). Differently from the deformation bands in glaciotectonic environment, which typically show a spread in strike direction, those associated with faulting follow the strike of the regional basement faults (Brandes et al., 2018b, 2022). Moreover, the cataclastic deformation bands indicate fault rupture processes (Cashman et al., 2007), whereas the non-cataclastic disaggregation bands decoupled from fluid escape structures serve as indicators of slow creeping (Brandes and Tanner, 2012; Brandes et al., 2022).

Altogether, we interpret the combination of large-scale slumping, water escape and load structures, clastic dykes and the shear deformation bands as generated by activity of deeper transtensional faults during repeated deformation episodes (Müller et al., 2021), most likely induced by seismic shocks (Fig. 13C). Moreover, the cyclic repetition of cross-cutting relationships between seismically-triggered SSDS and disaggregation bands (Fig. 13C) suggest the possible preservation of both the seismic and aseismic movements during syn-depositional deformation.

5.3. Implications for regional tectonics

Strikes of shear bands match the attitude of known large-scale faults faults in the underlying Briançonnais basement and in the Ligurian Sea offshore (Fig. 1; Boni et al., 1971; Vanossi et al., 1994; Maino et al., 2013; Decarlis et al., 2014; Morelli et al., 2022). Field-based structural investigations in the Ligurian Alps and Oligo-Miocene deposits of the Tertiary Piedmont Basin identified switch from extensional to transtensional regime in the Early Chattian (Maino et al., 2013). Since the Aquitanian, extensional and transpressional tectonics have been documented in both the Tertiary Piedmont Basin and the Ligurian Alps. They are interpreted as generated within a mega transtensional zone accommodating a regional rotation caused by the oceanic spreading of the Liguro-Provençal basin, the Corsica-Sardinia drifting and the eastward retreat of the Apenninic slab (Federico et al., 2009, 2014; Maino et al., 2013). Recent geophysical investigations along the margin of the Ligurian Sea provide evidence of Miocene to present-day active tectonic structures that experienced polyphasic evolution (Morelli et al., 2022). Two upper Miocene and Pliocene-Quaternary compressive events locally inverted the dominant Miocene to present extensional/transtensional tectonic trend. In the proximity of the Finale Ligure Basin, arrays of NE-SW trending faults, dissected by NW-SE-striking structures, characterize the Briançonnais basement in front of the Ligurian Sea (Fig. 1B). These faults show evidence of polyphasic evolution, ending with the dominantly transtensional kinematic. The new finding of co-seismic deformations in the shallow sediments allows constraining the activity of t deep faults in Langhian-Serravallian times. These faults accommodated multiple seismic input during the oceanic spreading of the Liguro-Provençal basin and the Corsica-Sardinia drifting.

6. Conclusions

This study explores a diverse assemblage of SSDS, distributed in lithologically disparate sediments of the mixed siliciclastic-carbonate Finale Ligure Basin. The SSD-prone interface between the terrigenous and carbonatic successions (i.e., the boundary between the *Basal complex of the Finale Ligure Limestone Fm.* and the *Finale Ligure Limestone Fm.*) is marked by abrupt lithological changes within short lateral distances. Here, we defined well-constrained stratigraphic intervals with SSDS featuring:

i) small size (cm to <1 m) load-and-flame structures, slumps, flame and pseudonodules, interpreted as resulting from overloading caused by a reversed density gradient.
ii) spectacular large-scale slumps, chaotic strata, sand intrusions, diapirs, dome and tree-like structures, interpreted to result from liquefaction of sandy beds limited by low-permeability beds. Large-size (up to 5 m high) water escape structures attest the expulsion of enormous volumes of overpressurized fluids, generating plastic and brittle deformation in their surrounding host rocks.
iii) SSDS display lateral continuity and sequential vertical and lateral organization. Arrays of deformation bands such as disaggregation and phyllosilicate dilational shear bands, carbonate filled veins and sandy dykelets accompany the cyclic repetition of these SSDs. Deformation bands display equal strike direction as the regional faults matching the orientation and the transtensional kinematic of the fault network described in the underlying basement both onshore and offshore the Ligurian margin. Their direct vicinity to water-escape SSDS supports the interpretation of an earthquake-induced origin. Moreover, the mutual crosscutting relationships between SSDS and shear bands suggest that both the seismic and slow creep movements are recorded by the deformed stratigraphic interval.
iv) Integrating both sedimentological and structural data reveals a seismogenic origin of assemblages of load-and-flame structures, ball-and-pillows, clastic injectites and shear deformation bands. Their concurrent presence potentially serves as a diagnostic tool for determining seismites. To validate this hypothesis more outcrop studies across various depositional environments in which this association is recorded are needed in order to verify the potential of this technique for the identification of earthquake-induced SSDS in the field.
v) The fact that SSDS resulting from earthquake-induced liquefaction and/or fluidization can confidentially be assigned to the Langhian-Serravallian interval makes them a suitable indicator of previously undocumented seismic pulses associated with the opening of the Liguro-Provençal Basin and the Corsica-Sardinia drifting.

Funding

This research was supported in the frame of the Italian 1:50.000 Geological Mapping project - CARG Foglio 245 - Albenga (ISPRA, Regione Liguria, University of Pavia and Genova).

Author contributions

MM and MP discovered the structures. MM and PM formulated the study conception and design with the contribution of ST, LC and LF. MP, PM, ST, MM, CA and NM performed the fieldwork. ST and PM prepared the samples, performed the stratigraphic/petrographic analysis and interpreted the relative data. NM acquired the orthophoto-panels and 3D Digital Outcrop Model (DOM) via drone imagery. NM, MP, ST and MM collected the structural data and defined their interpretation. SS and LC provided the project management and coordination. ST, PM, MP, NM provided the conceptualization, design and preparation of the figures. PM wrote the first draft of the manuscript and all authors commented on previous versions of the manuscript. All authors read and approved the final manuscript.

Declaration of competing interest

The authors declare the following financial interests/personal relationships which may be considered as potential competing interests: Matteo Maino reports financial support was provided by Institute for Environmental Protection and Research Department for the Geological Survey of Italy.

Data availability

Data will be made available on request.
https://skfb.ly/oDAYwLink
https://skfb.ly/oDAYJLink
https://skfb.ly/oDAZpLink
https://skfb.ly/oDC6J

Acknowledgment

We would like to express our gratitude to Maurizio Marino (Ispra) and Simone Fabbi (University of Rome “La Sapienza”) for the many fruitful discussion in the field and their constant support to the project. Marco Brandano is thanked for editorial handling. Massimo Moretti and the anonymous reviewer are thanked for helpful input that improved the clarity of the paper.

References

Alfaro, P., Delgado, J., Estévez, A., Molina, J.M., Moretti, M., Soria, J.M., 2002. Liquefaction and fluidization structures in messinian storm deposits of the lower segura basin (betic cordillera, southern Spain). International Journal of Earth Sciences/Geologische Rundschau 91, 505–513.
Allen, J.R.L., 1982. Sedimentary Structures: Their Character and Physical Basis, ume II. Elsevier, Amsterdam, The Netherland.
Alsop, G.I., Marco, S., Weinberger, R., Levi, T., 2016. Sedimentary and structural controls on seismogenic slumping within mass transport deposits from the Dead Sea Basin. Sediment. Geol. 344, 71–90.
Amadori, C., Maino, M., Marini, M., Casini, L., Carrapa, B., Jepson, G., Hayes, R.G., Nicola, C., Reguzzi, S., Di Giulio, A., 2023. The role of mantle upwelling on the thermal history of the Tertiary-Piedmont Basin at the Alps-Apennines tectonic boundary. Basin Res. https://doi.org/10.1111/bre.12752.
Bann, K.L., Fielding, C.R., 2004. An integrated ichnological and sedimentological comparison of non-deltaic shoreface and subaqueous delta deposits in Permian reservoir units of Australia. Geological Society, London, Special Publications 228, 273–310.
Baucon, A., Piazza, M., Cabella, R., Bonci, M.C., Capponi, L., de Carvalho, C.N., Briguglio, A., 2020. Buildings that ‘speak’: ichnological geoheritage in 1930s buildings in Piazza della Vittoria (Genova, Italy). Geoheritage 12 (70), 1–22. https://doi.org/10.1007/s12371-020-00496-x.
Berra, F., Felletti, F., 2011. Syndepositional tectonics recorded by soft-sediment deformation and liquefaction structures (continental Lower Permian sediments, Southern Alps, Northern Italy): stratigraphic significance. Sediment. Geol. 235 (3–4), 249–263. https://doi.org/10.1016/j.sedgeo.2010.08.006.
Bhattacharya, H.N., Bandyopadhyay, S., 1998. Seismites in a proterozoic tidal succession, singhbhum, Bihar, India. Sediment. Geol. 119, 239–252. https://doi.org/10.1016/S0037-0738(98)00051-7.
Boni, P., Mosna, S., Vanossi, M., 1968. La Pietra di Finale (Liguria occidentale). Atti dell’Istituto Geologico dell’Università di Pavia 18, 102–150.
Boni, A., Cerro, A., Gianotti, R., Vanossi, M., 1971. Note illustrative della Carta geologica d’Italia alla scala 1:100000, Foglio 92-93, albenga-savona. In: Serv. Geol. it., p. 142.
Bonini, L., Dallagiovanna, G., Seno, S., 2010. The role of pre-existing fault in the structural evolution of thrust systems: insights from the Ligurian Alps (Italy). Tectonophysics 480 (1–4), 73–87.
Bourli, N., Maravelis, A.G., Zelilidis, A., 2020. Classification of soft-sediment deformation in carbonates based on the lower cretaceous vigla formation, kastos, Greece. Int. J. Earth Sci. 109, 2599–2614. https://doi.org/10.1007/s00531-020-01919-4.
Brandano, M., Tomassetti, L., Virgilio Frezza, V., 2015. Halimeda dominance in the coastal wedge of Pietra di Finale (Ligurian Alps, Italy): the role of trophic conditions. Sediment. Geol. 320, 30–37.
Brandano, M., Tomassetti, L., Puce, S., 2022. Carbonate factory of Pietra di Finale coastal wedge (Miocene): the unusual abundance of stylasterids (Cnidaria, Hydrozoa). Facies 68, 14.
Brandes, C., Tanner, D.C., 2012. Three-dimensional geometry and fabric of shear deformation-bands in unconsolidated Pleistocene sediments. Tectonophysics 518, 84–92.
Brandes, C., Winsemann, J., Roskosch, J., Meinsen, J., Tanner, D.C., Frechen, M., Steffen, H., Wu, P., 2012. Activity along the osning thrust in central europe during the lateglacial: ice-sheet and lithosphere interactions. Quat. Sci. Rev. 38, 49–62.
Brandes, C., Winsemann, J., 2013. Soft-sediment deformation structures in NW Germany caused by Late Pleistocene seismicity. Int. J. Earth Sci. 102, 2255–2274.
Brandes, C., Steffen, H., Sandersen, P.B.E., Wu, P., Winsemann, J., 2018a. Glacially induced faulting along the NW segment of the Sorgenfrei-Tornquist Zone, northern Denmark: implications for neotectonics and Lateglacial fault-bound basin formation. Quat. Sci. Rev. 189, 149–168.

Brandes, C., Igel, J., Loewer, M., Tanner, D.C., Lang, J., Müller, K., Winsemann, J., 2018b. Visualisation and analysis of shear-deformation bands in unconsolidated Pleistocene sand using ground-penetrating radar: implications for paleoseismological studies. Sediment. Geol. 367, 135–145.
Brandes, C., Tanner, D.C., Fossen, H., Halisch, M., Müller, K., 2022. Disaggregation bands as an indicator for slow creep activity on blind faults. Communications Earth & Environment 3 (1), 99.
Brogi, A., Capezzuoli, E., Moretti, M., Olvera-García, E., Matera, P.F., Garduno-Monroy, V.H., Mancini, A., 2018. Earthquake-triggered soft-sediment deformation structures (seismites) in travertine deposits. Tectonophysics 745, 349–365.
Bryant, G., Miall, A., 2010. Diverse products of near-surface sediment mobilization in an ancient eolianite: outcrop features of the early Jurassic Navajo Sandstone. Basin Res. 22 (4), 578–590.
Carter, R.M., Norris, R.J., 1986. Redeposited conglomerates in a Miocene flysch sequence at blackmount, western southland, New Zealand. Sediment. Geol. 18, 289–319.
Chen, P., Min, M., Chen, Y., Wang, L., Li, Y., Chen, Q., 2019. Review of the biological and engineering aspects of algae to fuels approach. Int. J. Agric. Biol. Eng. 2, 1–30. https://doi.org/10.3965/j.issn.1934-6344.2009.04.001-030.
Chiarella, D., Longhitano, S.G., Tropeano, M., 2017. Types of mixing and heterogeneities in siliciclastic-carbonate sediments. Mar. Petrol. Geol. 88, 617–627.
Collinson, J.D., Mountney, N.P., Thompson, D.B., 2006. Sedimentary Structures, third ed. Terra Publishing, England.
Crespellani, T., Nardi, R., Simoncini, C., 1988. La liquefazione del terreno in condizioni sismiche. Zanichelli.
Crispini, L., Federico, L., Capponi, G., Spagnolo, C., 2009. Late orogenic transpressional tectonics in the «Ligurian Knot. Boll. Soc. Geol. Ital. 128 (2), 433–441.
Dallagiovanna, G., Gaggero, L., Maino, M., Seno, S., Tiepolo, M., 2009. U–Pb zircon ages for post-Variscan volcanism in the Ligurian Alps (Northern Italy). Journal of the Geological Society of London 166, 101–114.
Dallagiovanna, G., Maino, M., Mancin, N., Seno, S., Giacomini, F., 2010. Oligo-miocene tectonic evolution of the finalese area (ligurian alps, NW Italy). Rendiconti Online della Società Geologica Italiana 10, 39–40.
Dallagiovanna, G., Gaggero, L., Seno, S., Felletti, F., Mosca, P., Decarlis, A., Pellegrini, L., Poggi, F., Bottero, D., Mancin, N., Lupi, C., Bonini, L., Lualdi, A., Maino, M., Toscani, G., 2011. Note Illustrative Della Carta Geologica d'Italia Alla Scala 1: 50.000, Foglio 228 Cairo Montenotte. ISPRA - Regione Liguria, Litografia Artistica Cartografica s.r.l, p. 156.
Decarlis, A., Dallagiovanna, G., Lualdi, A., Maino, M., Seno, S., 2013. Stratigraphic evolution in the ligurian alps between variscan heritages and the alpine tethys opening: a review. Earth Sci. Rev. 125, 43–68.
Decarlis, A., Maino, M., Dallagiovanna, G., Lualdi, A., Masini, E., Seno, S., Toscani, G., 2014. Salt tectonics in the SWAlps (Italy-France): from rifting to the inversion of the European continental margin in a context of oblique convergence. Tectonophysics 636, 293e314.
Decarlis, A., Beltrando, M., Manatschal, G., Ferrando, S., Carosi, R., 2017. Architecture of the distal Piedmont-Ligurian rifted margin in NW Italy: hints for a flip of the rift system polarity. Tectonics 36, 2388–2406. https://doi.org/10.1002/2017TC004561.
Della Porta, G., Nembrini, M., Berra, F., Vertino, A., 2022. Facies character and skeletal composition of heterozoan carbonates in a high-energy confined embayment (Miocene, Finale Ligure Limestone, NW Italy). Sediment. Geol. 438, 106209.
de Voogd, B., Nicolich, R., Olivet, J.L., Fanucci, F., Burrus, J., Mauffret, A., 1991. First deep seismic reflection transect from the gulf of lions to sardinia (ECORS-crop profiles in western mediterranean). American Geophysical Union (AGU) 22, 265–274. https://doi.org/10.1029/gd022 p0265.
Du, X., Ye, M., Xie, X., Zhao, K., Jia, J., Du, X., 2022. Why is it easy to form high-quality reservoirs in a mixed siliciclastic-carbonate system? Evidence from diagenetic characteristics. J. Petrol. Sci. Eng. 212, 110339.
Ekwenye, O., Mode, A., Oha, I., Onah, F., 2020. Soft-sediment deformation in the campanian-maastrichtian deltaic deposits of the afikpo sub-basin, south-eastern Nigeria: recognition of endogenic trigger. Jordan Journal of Earth and Environmental Sciences 11 (1), 1–11.
Ettensohn, F.R., Zhang, C., Gao, L., Lierman, R.T., 2011. Soft-sediment deformation in epicontinental carbonates as evidence of paleoseismicity with evidence for a possible new seismogenic indicator: accordion folds. Sediment. Geol. 235 (3–4), 222–233.
Faccenna, C., Piromallo, C., Crespo-Blanc, A., Jolivet, L., Rossetti, F., 2004. Lateral slab deformation and the origin of the western Mediterranean arcs. Tectonics 23 (1).
Farrell, N.J.C., Healy, D., Taylor, C.W., 2014. Anisotropy of permeability in faulted porous sandstones. J. Struct. Geol. 63, 50–67.
Fattah, A., Abu Sharib, A.S.A.A., 2023. Liquefaction-induced structures, hammam faroun block, gulf of suez rift, Egypt: possible rift-related neogene seismites. Int. J. Earth Sci. 1–19.
Federico, L., Spagnolo, C., Crispini, L., Capponi, G., 2009. Fault-slip analysis in the metaophiolites of the Voltri Massif: constraints for the tectonic evolution at the Alps/Apennine boundary. Geol. J. 44 (2), 225–240. https://doi.org/10.1002/gj.1139.
Federico, L., Crispini, L., Vigo, A., Capponi, G., 2014. Unravelling polyphase brittle tectonics through multi-software fault-slip analysis: the case of the Voltri Unit, Western Alps (Italy). J. Struct. Geol. 68, 175–193.
Federico, L., Maino, M., Capponi, G., Crispini, L., 2020. Paleo-depth of fossil faults estimated from paleostress state: applications from the Alps and the Apennines (Italy). J. Struct. Geol. 140, 104152 https://doi.org/10.1016/j.jsg.2020.104152.
Fossen, H., Schultz, R.A., Shipton, Z.K., Mair, K., 2007. Deformation bands in sandstone: a review. J. Geol. Soc. 164, 755–769 (London).
Fossen, H., Soliva, R., Ballas, G., Trzaskos, B., Cavalcante, C., Schultz, R.A., 2018. A review of deformation bands in reservoir sandstones: geometries, mechanisms and distribution. Geological Society, London, Special Publications 459 (1), 9–33.
Galli, P., 2000. New empirical relationships between magnitude and distance for liquefaction. Tectonophysics 324 (3), 169–187.
Gattacceca, J., Deino, A., Rizzo, R., Jones, D.S., Henry, B., Beaudoin, B., Vadeboin, F., 2007. Miocene rotation of Sardinia: new paleomagnetic and geochronological constraints and geodynamic implications. Earth Planet Sci. Lett. 258 (3–4), 359–377. https://doi.org/10.1016/j.epsl.2007.02.003.
Giacomini: Unpublished MSc Thesis, 2009. University of Pavia.
Greb, S.F., Archer, A.W., 2007. Soft-sediment deformation produced by tides in a meizoseismic area, Turnagain Arm, Alaska. Geology 35 (5), 435–438.
Gruszka, B., van Loon, A.T., 2007. Pleistocene glaciolacustrine breccias of seismic origin in an active graben (central Poland). Sediment. Geol. 193 (1–4), 93–104.
Hargitai, H., Levi, T., 2014. Clastic dikes. In: Hargitai, H., Kereszturi, A. (Eds.), Encyclopedia of Planetary Landforms. Springer, New York, pp. 1–9.
Hickson, T.A., Lowe, D.R., 2002. Facies architecture of a submarine fan channel–levee complex: the Juniper Ridge Conglomerate, Coalinga, California. Sedimentology 49 (2), 335–362.
Hilbert-Wolf, H.L., Roberts, E.M., Simpson, E.L., 2016. New sedimentary structures in seismites from SW Tanzania: evaluating gas- vs. water-escape mechanisms of soft deformation. Sediment. Geol. 344, 253–262.
Horowitz, D.H., 1982. Geometry and origin of large-scale deformation structures in some ancient wind-blown sand deposits. Sedimentology 29, 155–180.
Hussain, A., Butt, M.N., Olariu, C., Malik, M.H., Koeshidayatullah, A., Amao, A., Al-Ramadan, K., 2022. Unravelling reservoir quality heterogeneity in mixed siliciclastic-carbonate deposits: an example from Miocene Red Sea rift, NW Saudi Arabia. Mar. Petrol. Geol. 145, 105850.
Issel, A., 1892. Liguria geologica e preistorica. 2 voll. Donath, Genova.
Kolbuszewski, J., Nadolski, L., Dydacki, Z., 1950. Porosity of wind-deposited sands. Geol. Mag. 87 (6), 433–435.
Kolbuszewski, J., 1953. Note on factors governing the porosity of wind deposited sands. Geol. Mag. 90 (1), 48–56.
Kolmar, P.D., Cui, B., 1984. The analysis of grain-size measurements by sieving and settling-tube techniques. J. Sediment. Res. 54 (2), 603–614.
Larroque, C., de Lépinay, B.M., Migeon, S., 2011. Morphotectonic and fault–earthquake relationships along the northern Ligurian margin (western Mediterranean) based on high resolution, multibeam bathymetry and multichannel seismic-reflection profiles. Mar. Geophys. Res. 32 (1–2), 163–179.
Le Heron, D.P., Sutcliffe, O.E., Whittington, R.J., Craig, J., 2005. The origins of glacially related softsediment deformation structures in Upper Ordovician glaciogenic rocks: implication for ice-sheet dynamics. Palaeogeogr. Palaeoclimatol. Palaeoecol. 218, 75–103.
Liesa, C.L., Rodríguez-Lopez, J.P., Ezquerro, L., Alfaro, P., Rodríguez-Pascua, M.A., Lafuente, P., Arlegui, L., Simon, J.L., 2016. Facies control on seismites in an alluvialeaeolian system: the Pliocene dune field of the Teruel half-graben basin (eastern Spain). Sediment. Geol. 344, 237–252.
Lowe, D.R., 1975. Water escape structures in coarse-grained sediments. Sedimentology 31, 749–754.
Maffione, M., Speranza, F., Faccenna, C., Cascella, A., Vignaroli, G., Sagnotti, L., 2008. A synchronous Alpine and Corsica-Sardinia rotation. J. Geophys. Res. Solid Earth 113, B03104. https://doi.org/10.1029/2007J B005214.
Main, I.G., Kwon, O., Ngwenya, B.T., Elphick, S.C., 2000. Fault sealing during deformation-band growth in porous sandstone. Geology 28 (12), 1131–1134.
Maino, M., Seno, S., 2016. The thrust zone of the ligurian penninic basal contact (Monte fronté, ligurian alps, Italy). J. Maps 12, 341–351.
Maino, M., Dallagiovanna, G., Dobson, K.J., Gaggero, L., Persano, C., Seno, S., Stuart, F. M., 2012. Testing models of orogen exhumation using zircon (U–Th)/He thermochronology: insight from the Ligurian Alps, Northern Italy. Tectonophysics 560–561, 84–93. https://doi.org/10.1016/j.tecto.2012.06.045.
Maino, M., Decarlis, A., Felletti, F., Seno, S., 2013. Tectono-sedimentary evolution of the tertiary Piedmont BasinBasin (NW Italy) within the oligo-miocene central mediterranean geodynamics. Tectonics 32 (3), 593–619. https://doi.org/10.1002/tect.20047.
Maino, M., Bonini, L., Dallagiovanna, G., Seno, S., 2015a. Large sheath folds in the Briançonnais of the Ligurian Alps reconstructed by analysis of minor structures and stratigraphic mapping. J. Maps 11 (1), 157–167.
Maino, M., Casini, L., Ceriani, A., Decarlis, A., Di Giulio, A., Seno, S., Setti, M., Stuart, F. M., 2015b. Dating shallow thrusts with zircon (U-Th)/He thermochronometry—the shear heating connection. Geology 43, 495–498. https://doi.org/10.1130/G36492.1.
Maino, M., Gaggero, L., Langone, A., Seno, S., Fanning, M., 2019. Cambro-silurian magmatisms at the northern gondwana margin (penninic basement of the ligurian alps). Geosci. Front. 10 (1), 315–330. https://doi.org/10.1016/j.gsf.2018.01.003.
Maino, M., Casini, L., Boschi, C., Di Giulio, A., Setti, M., Seno, S., 2020. Time-dependent heat budget of a thrust from geological records and numerical experiments. J. Geophys. Res. Solid Earth 125 (3). https://doi.org/10.1029/2019JB018940.
Maino, M., Adamuszek, M., Schenker, F.L., Seno, S., Dabrowski, M., 2021. Sheath fold development around deformable inclusions: integration of field-analysis (Cima Lunga unit, Central Alps) and 3D numerical models. J. Struct. Geol. 144, 104255.
Marshall, J.D., 2000. Sedimentology of a Devonian fault-bounded braidplain and lacustrine fi ll in the lower part of the Skrinkle Sandstones, Dyfed, Wales. Sedimentology 47, 325–342.
Martinsen, O.J., 1989. Styles of soft-sediment deformation on a namurian (carboniferous) delta slope, western Irish namurian basin, Ireland. Geological Society, London, Special Publications 41, 167–177.
Menegoni, N., Inama, R., Crozi, M., Perotti, C., 2022. Early deformation structures connected to the progradation of a carbonate platform: the case of the Nuvolau

Cassian platform (Dolomites-Italy). Mar. Petrol. Geol. 138, 105574 https://doi.org/10.1016/j.marpetgeo.2022.105574.
Mills, P.C., 1983. Genesis and diagenetic value of soft-sediment deformation structures - a review. Sediment. Geol. 35, 83–104.
Molenaar, N., Van de Bilt, G.P., Van den Hoek Ostende, E.R., Nio, S.D., 1988. Early diagenetic alteration of shallow-marine mixed sandstones: an example from the lower Eocene Roda sandstone member, Tremp-Graus basin, Spain. Sediment. Geol. 55 (29), 5–318.
Molina, J.M., Alfaro, P., Moretti, M., Soria, J.M., 1998. Soft-sediment deformation structures induced by cyclic stress of storm waves in tempestites (Miocene, Guadalquivir Basin, Spain). Terra. Nova 10, 145–150.
Montenat, C., Barrier, P., Ott d'Estevou, P., Hibsch, C., 2007. Seismites: an attempt at critical analysis and classification. Sediment. Geol. 196, 5–30.
Morelli, D., Martorelli, E., Casalbore, D., Chiocci, F.L., 2022. Morpho-stratigraphic evolution of a tectonically controlled canyon-channel system in the gioia basin (southern tyrrhenian Sea). Mar. Geol. 451, 106881.
Moretti, M., 2000. Soft-sediment deformation structures interpreted as seismites in middle-late Pleistocene aeolian deposits (Apulian foreland, southern Italy). Sediment. Geol. 135, 167–179.
Moretti, M., Sabato, L., 2007. Recognition of trigger mechanisms for soft-sediment deformation in the Pleistocene lacustrine deposits of the Sant'Arcangelo Basin (Southern Italy): seismic shock vs. overloading. Sediment. Geol. 196 (1–4), 31–45.
Moretti, M., Ronchi, A., 2011. Liquefaction features interpreted as seismites in the pleistocene fluvio-lacustrine deposits of the neuquén basin (northern patagonia). Sediment. Geol. 235 (3–4), 200–209.
Moretti, M., van Loon, A.J., Liu, M., Wang, Y., 2014. Restrictions to the application of 'diagnostic' criteria for recognizing ancient seismites. J. Palaeogeogr. 3 (2), 162–173.
Morsilli, M., Giona Bucci, M., Gliozzi, E., Lisco, S., Moretti, M., 2020. Sedimentary features influencing the occurrence and spatial variability of seismites (late Messinian, Gargano Promontory, southern Italy). Sediment. Geol. 401, 105628 https://doi.org/10.1016/j.sedgeo.2020.105628.
Mosna, S., Seno, S., Vanossi, M., 1990. Depositi post-orogeni dell'Oligocene Inferiore interposti tra il Brianzonese e la "Pietra di Finale" (Alpi Liguri): conseguenze paleotettoniche e paleogeografiche. Atti Tic. Sc. Terra 33, 11–21.
Müller, K., Winsemann, J., Pisarska-Jamroży, M., Lege, T., Spies, T., Brandes, C., 2021. The challenge to distinguish soft-sediment deformation structures (SSDS) formed by glaciotectonic, periglacial and seismic processes in a formerly glaciated area: a review and synthesis. In: Steffen, H., Olesen, O., Sutinen, R. (Eds.), Glacially-Triggered Faulting. Cambridge University Press, Cambridge, pp. 67–88. https://doi.org/10.1017/9781108779906.007.
Mueller, P., Maino, M., Seno, S., 2020. Progressive deformation patterns from an accretionary prism (helminthoid flysch, ligurian alps, Italy). Geosciences 10 (1), 26. https://doi.org/10.3390/geosciences10010026.
Mugnier, J.L., Huyghe, P., Gajurel, A.P., Upreti, B.N., Jouanne, F., 2011. Seismites in the Kathmandu basin and seismic hazard in central Himalaya. Tectonophysics 509 (1–2), 33–49.
Obermeier, S.F., 1996. Use of liquefaction induced features for paleoseismic analysis – an overview of how seismic liquefaction features can be distinguished from other features and how their regional distribution and properties of source sediment can be used to infer the location and strength of Holocene paleo-earthquakes. Eng. Geol. 44, 1–76.
Okusa, S., 1985. Wave-induced stresses in unsaturated submarine sediments. Geotechnique 35 (4), 517–532.
Oliveira, C.M., Hodgson, D.M., Flint, S.S., 2009. Aseismic controls on in situ soft-sediment deformation processes and products in submarine slope deposits of the Karo Basin, South Africa. Sedimentology 56, 1201–1225.
Oudet, J., Münch, P., Verati, C., Ferrandini, M., Melinte-Dobrinescu, M., Gattacceca, J., Cornée, J.J., Oggiano, G., Quillévéré, F., Borgomano, J., Ferrandini, J., 2010. Integrated chronostratigraphy of an intra-arc basin: 40Ar/39Ar datings, micropalaeontology and magnetostratigraphy of the early Miocene Castelsardo basin (northern Sardinia, Italy). Palaeogeogr. Palaeoclimatol. Palaeoecol. 295 (1–2), 293–306.
Owen, G., 1987. Deformation processes in unconsolidated sands. In: Jones, M.E., Preston, R.M.F. (Eds.), Deformation of Sediments and Sedimentary Rocks, vol. 29. Geological Society, London, Special Publication, pp. 11–24.
Owen, G., 2003. Load Structures: Gravity Driven Sediment Mobilization in the Shallow Subsurface, vol. 216. Geological Society of London, Special Publication, pp. 21–34.
Owen, G., Moretti, M., 2008. Determining the origin of soft-sediment deformation structures: a case study from Upper Carboniferous delta deposits in south-west Wales, UK. Terra. Nova 20, 237–245.
Owen, G., Moretti, M., 2011. Identifying triggers for liquefaction induced soft-sediment deformation in sands. Sediment. Geol. 235, 141–147.
Owen, G., Moretti, M., Alfaro, P., 2011. Recognising triggers for soft-sediment deformation: current understanding and future directions. Sediment. Geol. 235, 133–140.
Peters, S.E., Loss, D.P., 2012. Storm and fair-weather wave base: a relevant distinction? Geology 40 (6), 511–514.
Rabbani, A., Assadi, A., Kharrat, R., Dashti, N., Ayatollahi, S., 2017. Estimation of carbonates permeability using pore network parameters extracted from thin section images and comparison with experimental data. J. Nat. Gas Sci. Eng. 42, 85–98.
Rasband, WS., ImageJ, U.S. National Institutes of Health, Bethesda, Maryland, USA, imagej.nih.gov/ij/, 1997–2012.
Ricci Lucchi, F., 1995. Sedimentographica. A Photographic Atlas of Sedimentary Structures, second ed. Columbia University Press, New York, p. 280.
Rodrigues, N., Cobbold, P.R., Løseth, H., 2009. Physical modelling of sand injectites. Tectonophysics 474 (3–4), 610–632.
Rodríguez-Pascua, M.A., Calvo, J.P., De Vicente, G., Gómez-Gras, D., 2000. Soft-sediment deformation structures interpreted as seismites in lacustrine sediments of the Prebetic Zone, SE Spain, and their potential use as indicators of earthquake magnitudes during the Late Miocene. Sediment. Geol. 135, 117–135.
Rollet, N., Déverchère, J., Beslier, M.O., Guennoc, P., Réhault, J.P., Sosson, M., Truffert, C., 2002. Back arc extension, tectonic inheritance, and volcanism in the Ligurian Sea, Western Mediterranean. Tectonics 21 (3). https://doi.org/10.1029/2001T C900027, 6-1–6-23.
Rossetti, D.F., Góes, A.M., 2000. Deciphering the sedimentological imprint of paleoseismic events: an example from the Aptian Codo Formation, northern Brazil. Sediment. Geol. 135 (1–4), 137–156.
Rudersdorf, A., Hartmann, K., Yu, K., Stauch, G., Reicherter, K., 2015. Seismites as indicators for holocene seismicity in the northeastern ejina basin, inner Mongolia. In: Landgraf, A., Kübler, S., Hintersberger, E., Stein, S. (Eds.), Fault Rupture and Earthquake Hazards in Slowly Deforming Regions, vol. 432. Geological Society, London, Special Publications, pp. 213–231.
Seilacher, A., 1969. Fault-graded beds interpreted as seismites. Sedimentology 13, 155–159.
Seno, S., Dallagiovanna, G., Vanossi, M., 2003. Palaeogeography and thrust development in the penninic domain of the western alpine chain: examples from the ligurian alps. Boll. Soc. Geol. Ital. 122 (2), 223–232.
Seno, S., Dallagiovanna, G., Vanossi, M., 2005. A kinematic evolutionary model for the Penninic sector of the central Ligurian Alps. Int. J. Earth Sci. 94, 114–129.
Shanmugam, G., 2017. Global case studies of soft-sediment deformation structures (SSDS): definitions, classifications, advances, origins, and problems. J. Palaeogeogr. 6 (4), 251–320. https://doi.org/10.1016/j.jop.2017.06.004.
Scholz, H., Frieling, D., 2006. Wulstgefüge, Rutschfalten und Sandsteingänge in Molassesedimenten – hinweise aus seismische Unruhe im Oligozän und Miozän des Alpenvorlands. Molasse sediments with ball-and-pillows, slumping structures and clastic dykes – indication on seismic unrest within the Oligocene and Miocene of the Alpine Foreland. Neues Jb. Geol. Paläontol. Abh. 241, 345–382.
Smellie, J.L., McArthur, J.M., McIntosh, W.C., Esser, R., 2006. Late neogene interglacial events in the james ross island region, northern antarctic peninsula, dated by Ar/Ar and Sr-isotope stratigraphy. Palaeogeogr. Palaeoclimatol. Palaeoecol. 242 (3–4), 169–187.
Speranza, F., Villa, I.M., Sagnotti, L., Florindo, F., Cosentino, D., Cipollari, P., Mattei, M., 2002. Age of the corsica–sardinia rotation and liguro–provençal basin spreading: new paleomagnetic and Ar/Ar evidence. Tectonophysics 347 (4), 231–251.
Sternlof, K.R., Chapin, J.R., Pollard, D.D., Durlofsky, L.J., 2004. Permeability effects of deformation band arrays in sandstone. AAPG Bull. 88 (9), 1315–1329.
Twiss, R.J., Moores, E.M., 1992. Structural Geology. Macmillan.
Van Loon, A.J., 2009. Soft-sediment deformation structures in siliciclastic sediments: an overview. Geologos 15, 3–55.
Van Loon, A.J., Pisarska-Jamroży, M., 2014. Sedimentological evidence of Pleistocene earthquakes in NW Poland induced by glacio-isostatic rebound. Sediment. Geol. 300, 1–10.
Van Loon, A.J., Pisarska- Jamroży, M., Woronko, B., 2020. Sedimentological distinction in glacigenic sediments between load casts induced by periglacial processes from those induced by seismic shocks. Geol. Q. 64 (3), 626–640.
Vanossi, M., Perotti, C.R., Seno, S., 1994. The maritime alps arc in the ligurian and tyrrhenian systems. Tectonophysics 230 (1–2), 75–89. https://doi.org/10.1016/0040-1951(94)90147 -3.
Vanossi, M., 1991. Guide Geologiche Regionali - Alpi Liguri (A Cura Della Societa' Geologica Italiana). BEMA Ed., p. 293
Vanossi, M., Cortesogno, L., Galbiati, B., Messiga, B., Piccardo, G.B., Vannucci, R., 1986. Geologia delle Alpi Liguri: dati, problemi, ipotesi. Memor. Soc. Geol. Ital. 28, 5–75.
Varejão, F.G., Warren, L.V., Simões, M.G., Cerri, R.I., Alessandretti, L., Santos, M.G.M.D., Assine, M.L., 2022. Evaluation of distinct soft-sediment deformation triggers in mixed carbonate-siliciclastic systems: lessons from the Brazilian Pre-Salt analogue Crato Formation (Araripe Basin, NE Brazil). Mar. Petrol. Geol. 140, 105673.
Vitale et al., 2018.
Warsitzka, M., Kukowski, N., May, F., 2017. Fluid-overpressure driven sediment mobilisation and its risk for the integrity for CO2 storage sites – an analogue modelling approach. Energy Proc. 114, 3291–3304. https://doi.org/10.1016/j.egypro.2017.03.1461.
Wegner, S., Stannarius, R., Boese, A., Rose, G., Szabo, B., Somfai, E., Börzsönyi, T., 2014. Effects of grain shape on packing and dilatancy of sheared granular materials. Soft Matter 10 (28), 5157–5167.
Went, D.J., 2005. Pre-vegetation alluvial fan facies and processes: an example from the cambro-ordovician rozel conglomerate formation, Jersey, channel islands. Sedimentology 52, 693–713.